Soil & Tillage Research 246 (2025) 106312

Contents lists available at ScienceDirect

Soil & Tillage Research

journal homepage: www.elsevier.com/locate/still

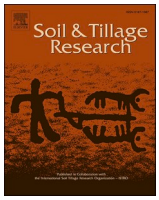

Integration soil contact model – A flexible pressure-sinkage method for simulating low speed vehicles with wheels and tracks

S. Kulju [a,*], J. Ala-Ilomäki [b]

[a] Natural Resources Institute Finland (Luke), Tekniikankatu 1, Tampere 33720, Finland
[b] Natural Resources Institute Finland (Luke), Latokartanonkaari 9, Helsinki 00790, Finland

ARTICLE INFO

Keywords:
Vehicle-terrain interaction
Physics-based simulation
Wheel
Tracks
Pressure-sinkage
Rolling resistance coefficient

ABSTRACT

An integration soil contact model and a modular terramechanics simulator VieteriSim for vehicles running on wheels and tracks were developed. The presented computational method extends the soil contact model by introducing a user defined pressure-sinkage relationship according to a theoretical function or an experimental data set, a numerical integration of pressure over a contact area with a desired resolution and vector based rolling resistance coefficient calculation. The convergence of the model and the capability of the computational method are demonstrated by simulating a cut-to-length timber forwarder running on a soft terrain with and without bogie tracks.

1. Introduction

Vehicles driving on soft terrain and wheel–soil interaction have been widely researched experimentally (Lamandé and Schjønning, 2011; Klaes et al., 2016; Salmivaara et al., 2018) and by simulations (Li and Sandu, 2007; Agarwal et al., 2019; El-Sayegh et al., 2020). The vehicle–terrain interaction is an interesting topic from multiple perspectives. The question may be looked from the point of view of the vehicle, providing for investigation of the trafficability of wheeled (Smith et al., 2014) or tracked vehicles (Perkins and Ma, 2002). Contrastingly, in the forests and agricultural fields, a pressure distribution and soil compaction (Keller et al., 2014; Keller and Arvidsson, 2016) or rut depths and rolling resistance coefficients (Kurjenluoma et al., 2009) on different terrains may be the main aspect.

The interaction between the wheels or tracks of the vehicle and the terrain have been computationally modeled with various methods. Pressure-sinkage models describe the response from the terrain with a function, which provides the resisting pressure generated by the terrain with given sinkage (Meirion-Griffith and Spenko, 2013). In the discrete element method, the soil is represented by a large number of discrete particles (Johnson et al., 2015; Wakui and Terumichi, 2011) and in the finite element method the terrain is represented by volumetric subparts (Li and Schindler, 2013; Taheri et al., 2015).

Schäfer et al. (2010) presented a soil contact model (SCM) for simulating Mars-rovers, and it is based on the pressure-sinkage model developed by Bekker (1969). A SCM was also used by Zhou et al. (2014) in Artemis (Adams-based Rover Terramechanics and Mobility Interaction Simulator) software, which was developed in a collaborative project of Washington University in St. Louis, California Institute of Technology and Massachusetts Institute of Technology.

In this article, we present the integration soil contact model (ISCM), an extension to the previously discussed SCM, and a modular simulation environment VieteriSim (Vehicle-Terrain Interaction Simulator), which was coded with the Python programming language. The ISCM relies on the numerical integration of the pressure over contact areas where the vehicle and the surface of the terrain are interacting. It also features a vector-based computation method for a rolling resistance coefficient calculation. Because of the computational nature of the ISCM, a pressure-sinkage relationship can be defined flexibly by a theoretical function or as an experimental data set and multiple pressure-sinkage relationships with varying locations can be used to achieve spatial variance.

2. Methods

The main principles of the simulator and the computation methods are presented in the following sections. The first subsection considers the modular generation of the 3D model of the vehicle and is followed by definitions of the geometry and the pressure-sinkage relationship of the terrain.

* Corresponding author.
E-mail address: sampo.kulju@luke.fi (S. Kulju).

https://doi.org/10.1016/j.still.2024.106312
Received 11 January 2024; Received in revised form 17 July 2024; Accepted 19 September 2024
Available online 18 October 2024

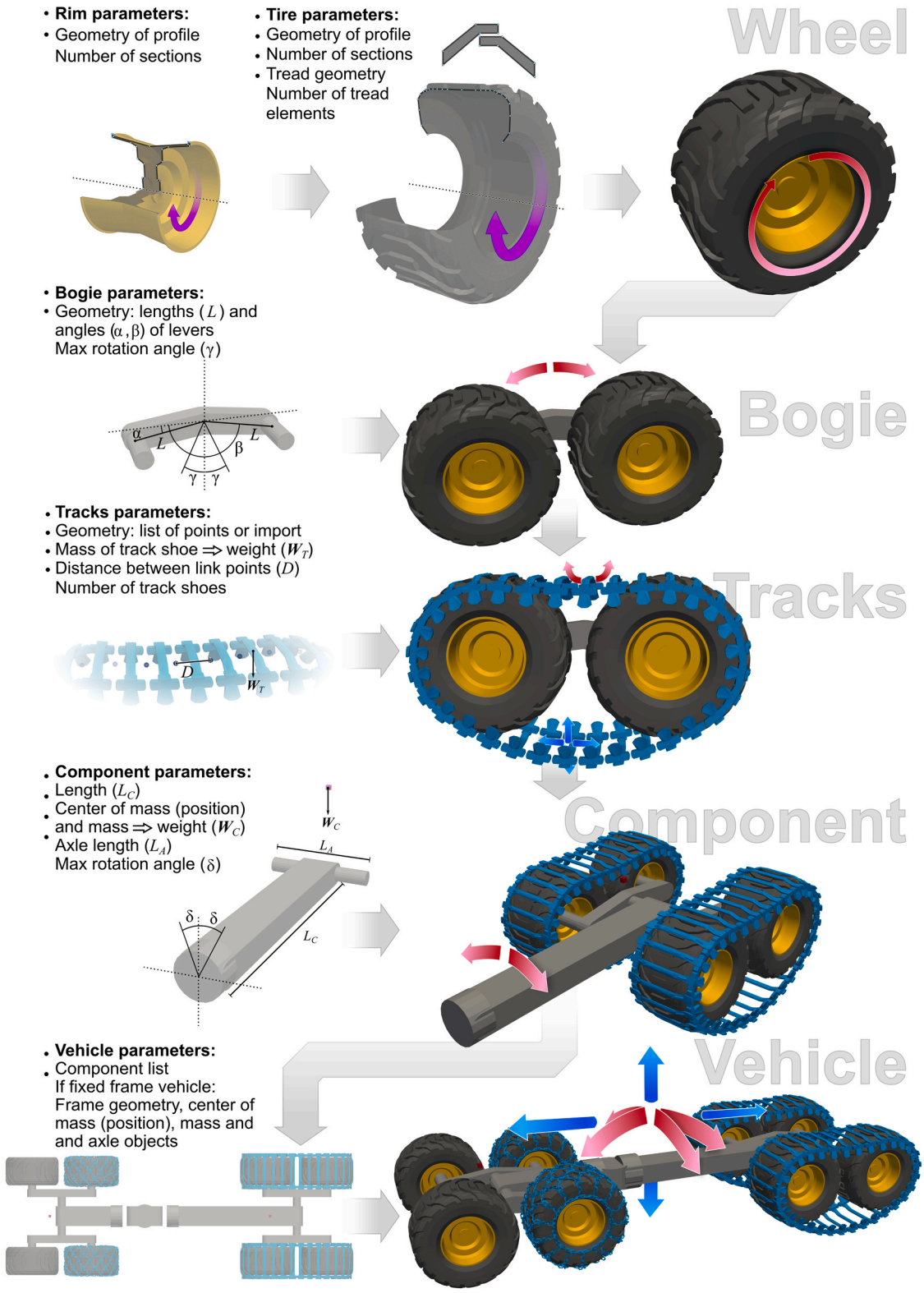

Fig. 1. Modular construction of the cut-to-length timber forwarder for simulations. Arrows present the degrees of freedom for each part type – red: rotation, blue: translation.

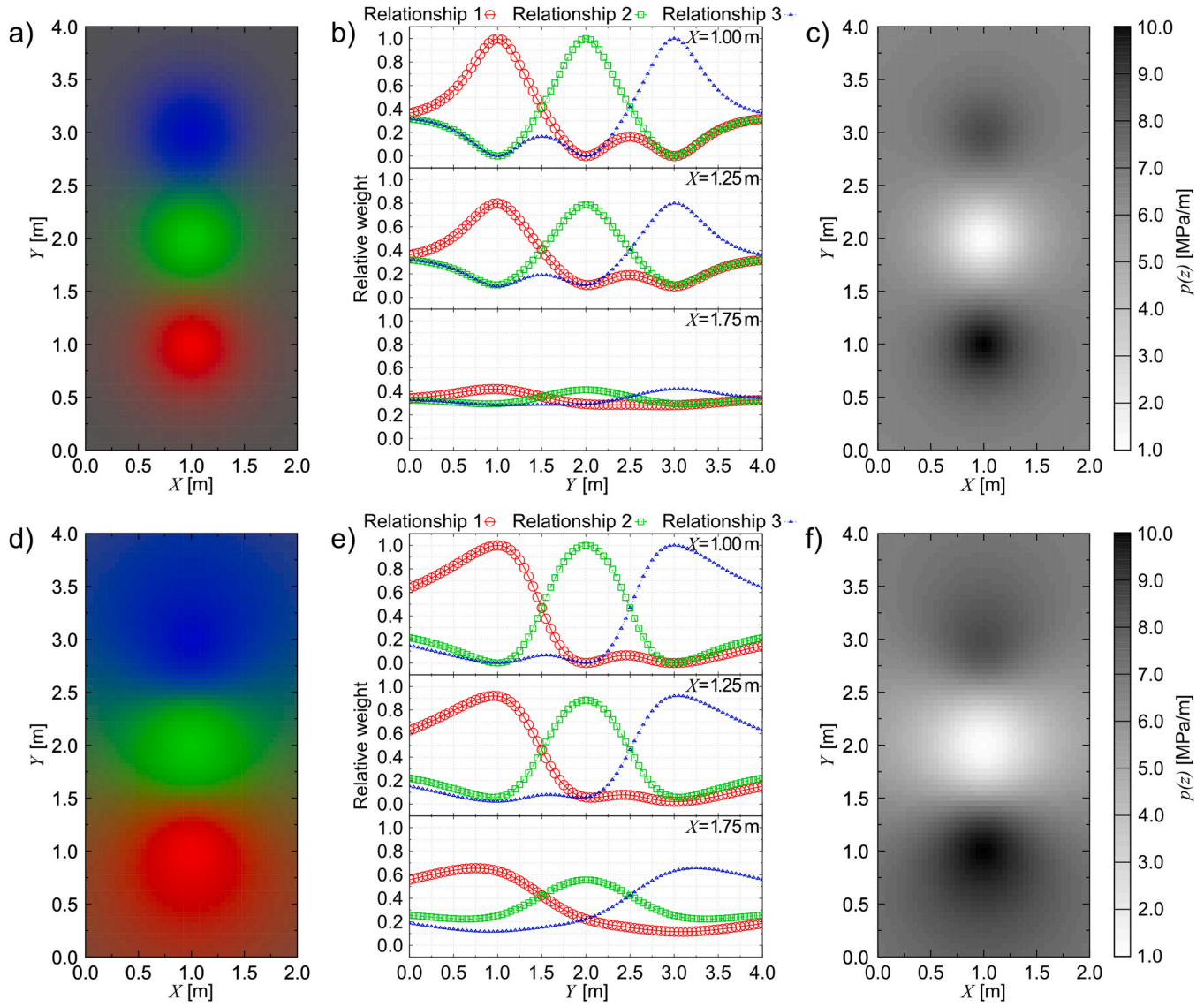

Fig. 2. The effect of the standard deviation, c, to the averaged pressure-sinkage relationship. Three linear pressure-sinkage relationships were defined as an initial input; 1) 10.0 MPa/m at position (1.0 m, 1.0 m), 2) 1.0 MPa/m at position (1.0 m, 2.0 m) and 3) 8.5 MPa/m at position (1.0 m, 3.0 m). Subfigure a) illustrates the relative weight values in RGB-space ($c = 0.5$ m), b) presents the relative weight values of each pressure-sinkage relationship from three cross-sections in subfigure a): $X = 1.00$ m, $X = 1.25$ m and $X = 1.75$ m and c) shows the final averaged pressure-sinkage relationship over the area ($c = 0.5$ m). Subfigures d), e) and f) present similar visualizations with $c = 1.5$ m.

After this the computational method for the vehicle–terrain interaction is described. The section covers the conversion of the 3D model of the vehicle to a grid defined by the digital elevation map (DEM) of the terrain surface, numerical integration of the pressure over the contact area to calculate acting forces and the optimization of the positions of tracks and vehicle components to find the final equilibrium and to calculate a rolling resistance coefficient. The last subsection considers the effects of run steps to simulated rut depths and to the rolling resistance coefficient.

This article presents multiple figures containing renderings of 3D models. During the simulation, the 3D model of the current state of the run, featuring geometries of the vehicle and the terrain surface, can be exported from the simulator in Visualization Toolkit (VTK) file format (Schroeder et al., 2006). These 3D scenes were visualized with the ParaView open-source interactive visualization software (Ahrens et al., 2005).

2.1. Modular generation of the vehicle

For simulation the vehicle geometry is described as a 3D model. Models for wheels and tracks can be generated in the simulator software according to simple inputs from the user. The 3D geometry of a track section can be also imported from a X3D-file. The parts of the vehicle chassis, such as bogies, axles and vehicle components and their parameters, for example dimensions, masses and maximum turning angles, are always defined by user input. The vehicle can be constructed from selected parts modularly. As an example, the construction of the cut-to-length timber forwarder for simulations is presented in this section and visualized in Fig. 1.

The modular construction of the cut-to-length timber forwarder is started by generating the wheel. The user defines cross section geometries of the rim and the tire by providing lists of points. These geometries are used as an input for a lathe-type function in which the user can define the wanted number of sectors to form 3D models.

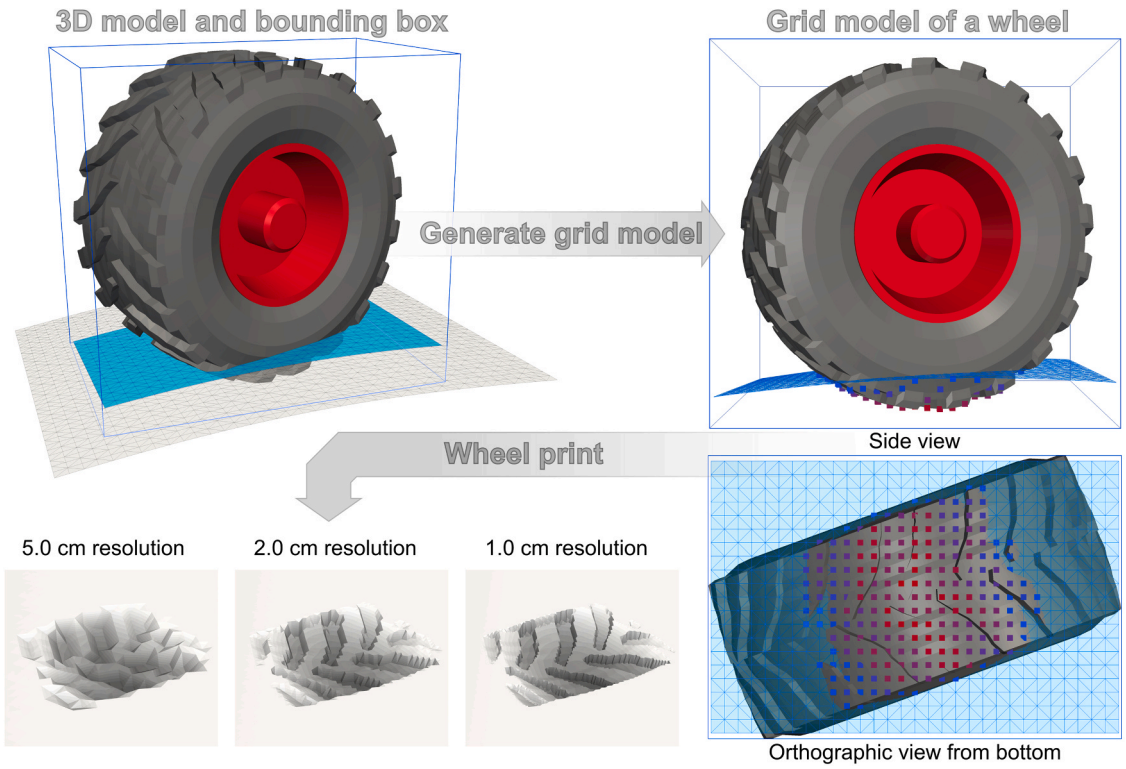

Fig. 3. Conversion from a 3D model to a grid model. The grid model of the wheel is presented with square dots colored according to their sinkage (blue: low – red: high). A smaller spatial resolution for a terrain surface is causing a finer print as presented by the examples.

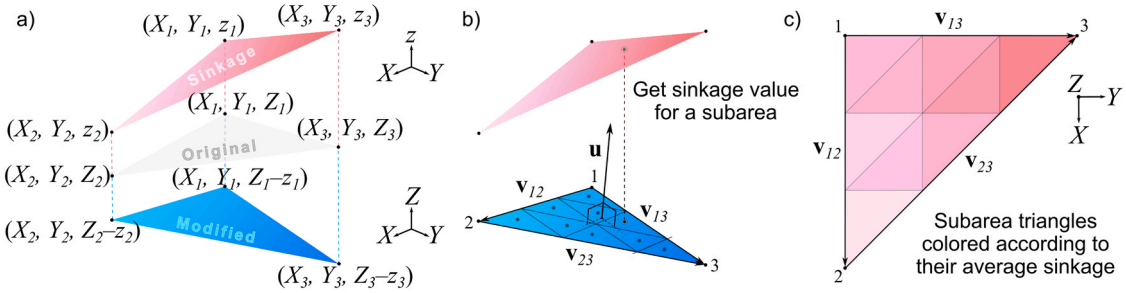

Fig. 4. The polygon formed by vertices defined in the surface array: a) original (unperturbed), modified (after load) and the same polygon in sinkage-space, b) subarea triangles of modified polygon and sinkage value designation for a subarea, c) subarea triangles colored according to their sinkage values (sinkage increases with darker color). Z_i, ($i = 1$–3) is the vertical component of the global coordinate in the real space, z_i is the vertical component for the sinkage space, and thus $Z_i - z_i$ is the vertical component of the vertex of the modified polygon in the real space. $\mathbf{v}_{12}$ is the vector from point 1–2, etc. and $\mathbf{u}$ is a unit vector perpendicular to the polygon surface.

After that, tread can be added to the tire. The user defines the tread geometry, including the height and the number of tread elements on the tire. The software converts the geometry of the tread to the grid defined by the points on the surface of the tire. By this manner, the points on tread elements, which can be thought to be solid and firm, can be linked to the points on the surface of the tire carcass. Thus, flexible tires with firm tread on rigid rims can be achieved in future versions of VieteriSim software.

The generated wheel object can be a part of a bogie, whose configurable parameters are presented in Fig. 1. A wheel or a bogie can also be equipped with tracks. Examples presented in this article cover only cases with metal tracks, thus they are defined by the geometry of the track shoe, the mass of the track shoe, the number of them and the track link pitch. However, the computational methods described in section 2.3 are also applicable to rubber tracks. If the tracks are on a single wheel, like chains in front bogies of the cut-to-length timber forwarder in Fig. 1, they are tightly fitted around the wheel and their geometry is not flexible and thus not optimized during the simulation. Bogies are finally attached to axles in components, defining the final geometry of the cut-to-length timber forwarder.

2.2. Terrain model

The model of a terrain is described with two arrays: a terrain surface array and a pressure-sinkage relationship array. Their features and definitions are presented in following sections.

2.2.1. Terrain surface

The terrain surface array consists of the parameters to define the surface topography and its current state. The geometry of the surface is

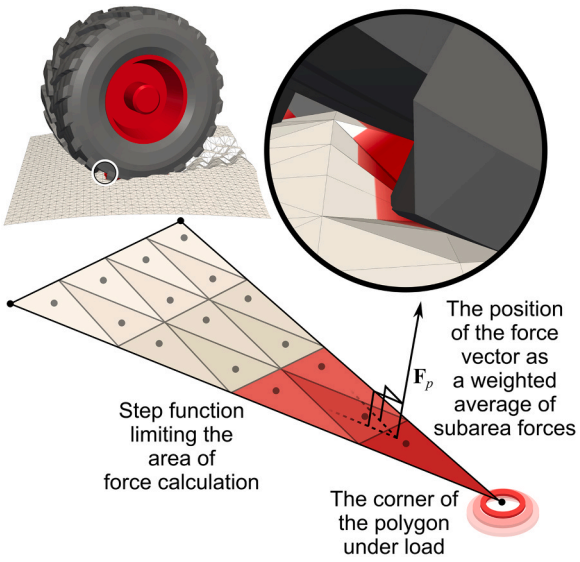

Fig. 5. The polygon under partial load. The force calculation is limited with a step function (calculated over subareas with red color).

described by a DEM with a spatial resolution in a centimeter scale. Thus, the surface array has global X, Y and Z-coordinates for each surface point. In addition to these, the array consists of a sinkage value and terrain type information for all the points. There are two terrain types:

1. Normal: The pressure response of the point is set by the pressure-sinkage relationship and the height (Z-coordinate) and sinkage values are modified during a simulation.
2. Fixed: The pressure-sinkage relationship of the point is predefined linear response and the height is fixed. This type is used for rigid objects on terrain, such as rocks and stumps.

The DEM for a surface can be imported or generated in the simulator, which provide functions for slopes, steps and sinusoidal waves, and the sum of them. There is also possibility to add rigid objects with desired diameters and heights.

Points in the surface array with their global coordinates are used as vertices for surface polygons. Polygons are formed by triangulating the DEM-defined rectangular 2D grid.

2.2.2. *Pressure-sinkage relationship*

The pressure-sinkage relationship defines the amount of pressure p, affecting an object when it has sank a distance z to a terrain. It can be described by a function or as an external input data. For the pressure-sinkage function $p(z)$ the only limitation is that it has to be defined for all sinkage values z, in an interval $[0, z_{max}]$, where z_{max} is an user defined maximum sinkage. In the case of the external data set, there are no limitations. However, in this case the maximum sinkage is defined by the maximum depth of the input data set.

For computation, the given pressure-sinkage relationship is converted to the pressure-sinkage array which defines the relationship for each surface point with a user-set sinkage resolution. For example, with 5.0 mm resolution, the pressure-sinkage relationship vector of a single terrain surface point is

$$\mathbf{p} = \langle p_0, p_5, p_{10}, \ldots, p_{zmax} \rangle, \quad (1)$$

where $p_0 = 0.0$ MPa, p_5 is pressure with 5.0 mm sinkage, and so on. Because pressure-sinkage relationships are defined in a discretized form, the pressure for the sinkage between the resolution set values is computed with a linear interpolation during the simulation.

Terrain with varying soil strength, for example a forest soil, can be

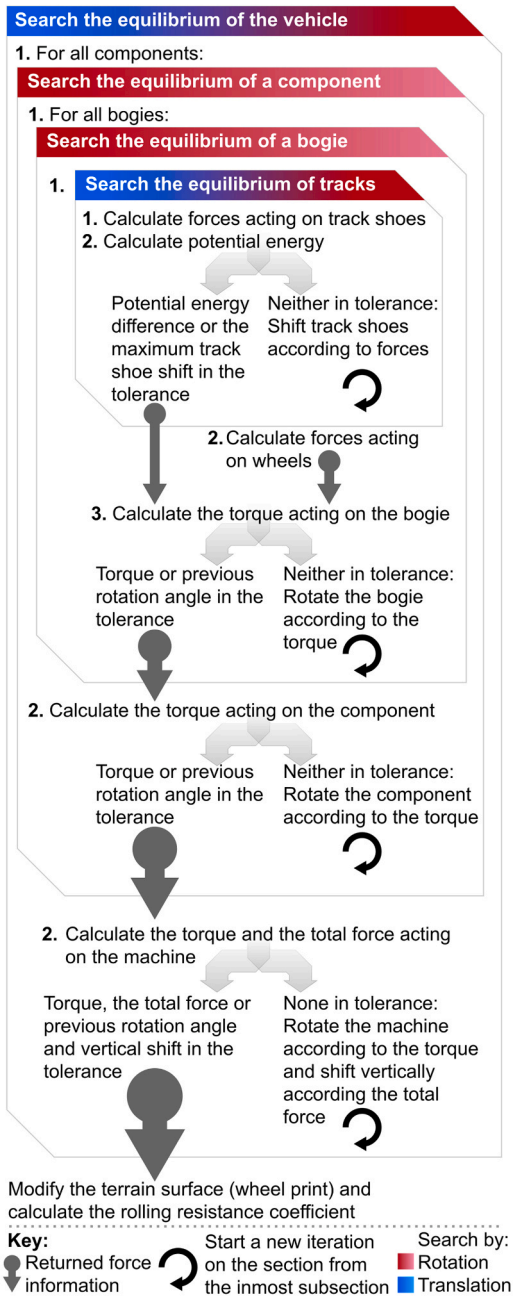

Fig. 6. Schematic flow chart of the equilibrium search for a vehicle with rotating components, such as the cut-to-length timber forwarder presented in Fig. 1.

described with a group of data sets (such as penetrometer measurements) or functions. In this case the positions of the measurements have to be provided. The simulator generates the weight of each given pressure-sinkage relationship for each surface point.

If there are pressure-sinkage relationships (data sets or functions) from M different positions and their position vectors in the XY-plane are $\{\mathbf{r}_1, \mathbf{r}_2, \ldots, \mathbf{r}_M\}$ relative to the origin of the terrain surface of the simulation, the absolute weight values for the terrain surface point S for each pressure-sinkage relationship are $\{w_{S1}, w_{S2}, \ldots, w_{SM}\}$. The absolute weight value of the pressure-sinkage relationship i for the terrain surface point S is

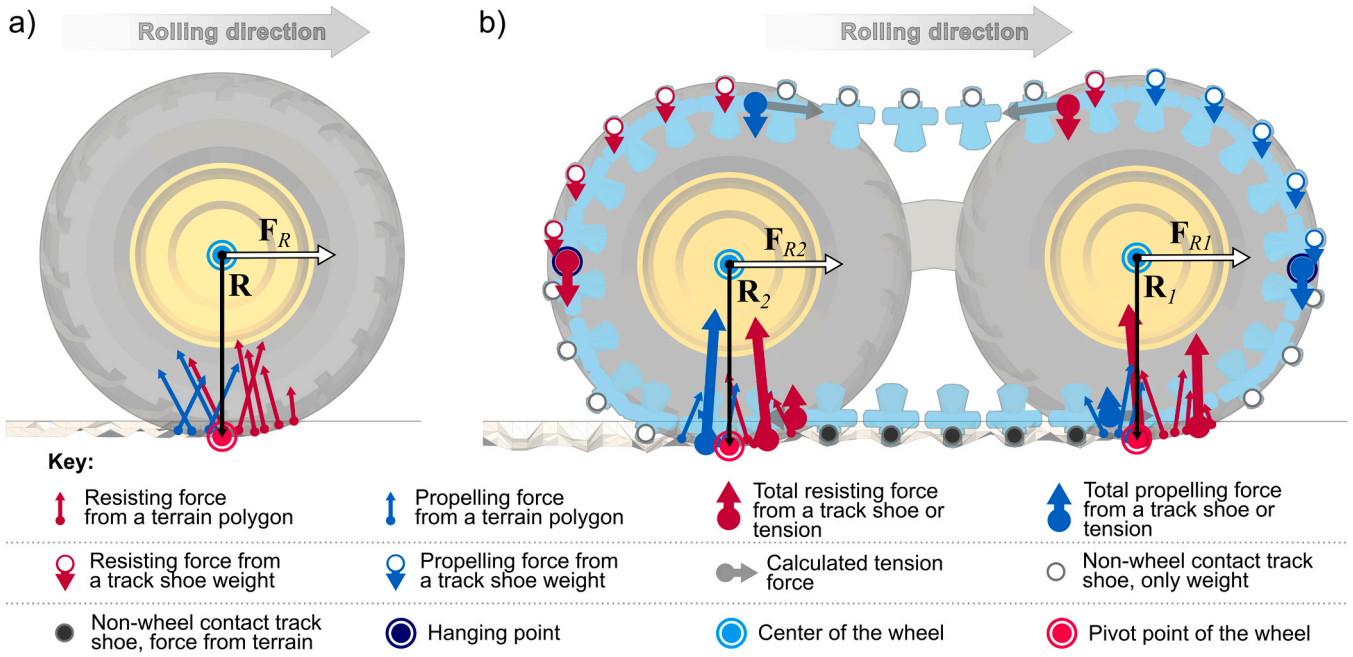

Fig. 7. Points, vectors and forces relevant for rolling resistance calculation. Examples given for a wheel (a) and a bogie with a tracks which partially covers the two tires (b).

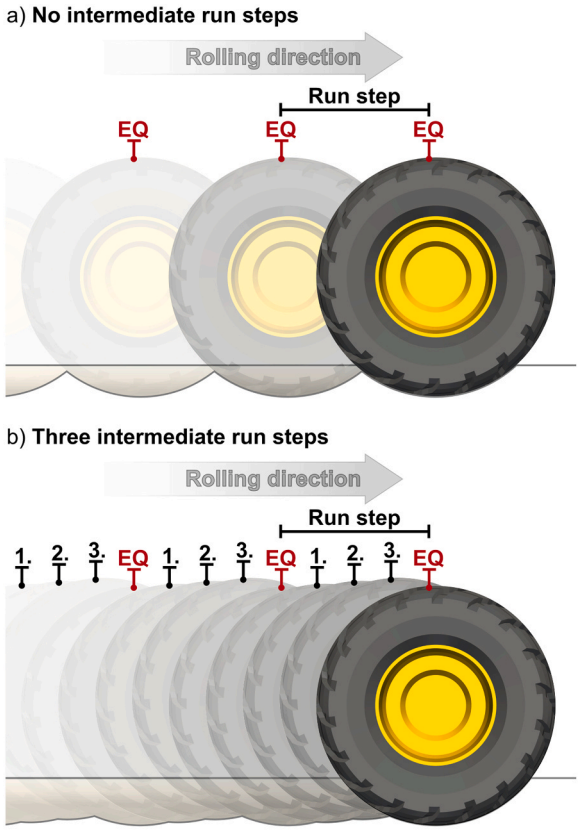

Fig. 8. A schematic image about the effect of intermediate steps to a rut depth with a single wheel running over a terrain.

$$w_{Si} = \prod_{k \neq i}^{M} \left(1 - \underbrace{\exp\left(-\frac{\| \mathbf{r}_k - \mathbf{r}_S \|^2}{2 \cdot c^2} \right)}_{G} \right), \tag{2}$$

where $\mathbf{r}_k$ is the position vector (in the XY-plane) for the pressure-sinkage relationship k, $\mathbf{r}_S$ is the position vector of the point S and c is the standard deviation of the Gaussian function G and this way the width of the bell curve. A threshold value $5 \cdot c$ was used as the maximum for distance $\|\mathbf{r}_k - \mathbf{r}_S\|$. For distances larger than the threshold value, the Gaussian function G was replaced simply by zero to prevent numerical errors. The pressure-sinkage relationship vector of the point S is then the weighted average of given pressure-sinkage relationships

$$\mathbf{p}_S = \frac{\sum_i^M w_{Si} \mathbf{p}_i}{\sum_i^M w_{Si}}, \tag{3}$$

where w_{Si} is the absolute weight value for pressure-sinkage relationship i calculated for the point S and $\mathbf{p}_i$ is the pressure-sinkage relationship i discretized to the vector form (Eq. (1)).

This approach automatically produces the even weighted average of pressure-sinkage relationships for surface points which are far from given input relationships. In addition, for points very close to the location of an input relationship, an effect from other input values is negligible.

The effect of the standard deviation c to the averaged pressure-sinkage relationship is presented in Fig. 2, where two different c values 0.5 m and 1.5 m were used. The pressure-sinkage array was generated for an area covering 2.0 m times 4.0 m with a spatial resolution of 0.05 m. Three linear pressure-sinkage relationships were defined as an initial input; 1) 10.0 MPa/m at position (1.0 m, 1.0 m), 2) 1.0 MPa/m at position (1.0 m, 2.0 m) and 3) 8.5 MPa/m at position (1.0 m, 3.0 m). For visualization purposes, the relative fraction of each weight value from the total sum of weight values is presented. Fig. 2 a) illustrates the relative weight values in RGB-space with $c = 0.5$ m, Fig. 2 b) presents the relative weight values of each pressure-sinkage relationship from three cross-sections in Fig. 2 a): $X = 1.00$ m, $X = 1.25$ m and $X = 1.75$ m, and Fig. 2 c) shows the final averaged pressure-sinkage

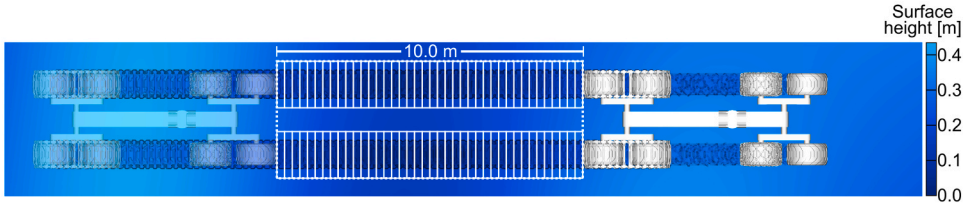

Fig. 9. The surface of the terrain after a single pass from the cut-to-length timber forwarder. The starting and final positions of the forwarder are visualized. Rut depths were measured from the left and right track by sampling the rut with a 25 centimeters long window and taking a maximum sinkage in the window for a rut depth value. These windows are presented with rectangular areas over ruts. Collection of rolling resistance coefficient value is started when the forwarder was fully inside the presented 10.0 m long area and was continued to the end of the run.

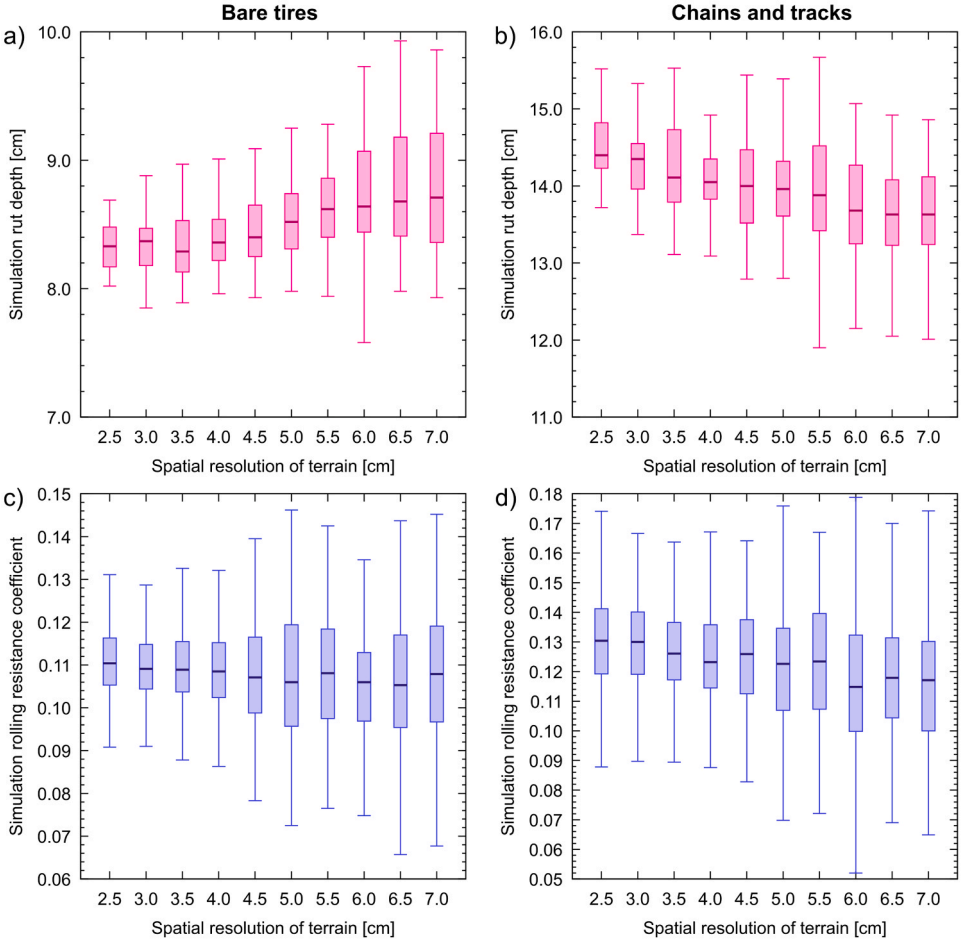

Fig. 10. Distributions of rut depth and rolling resistance coefficient for the Ponsse Elk forwarder on terrain surfaces with spatial resolution values in the 2.5 – 7.0 cm range. Values for the configuration running on bare tires are presented in a) and c) and the configuration with chains and tracks in b) and d).

relationship over the area. Fig. 2 d), e) and f) present the same visualizations for $c = 1.5$ m. Absolute weight values for the same cross-sections with both c values are presented in the Appendix, section A.

Rigid objects, such as rocks and stumps are identified in the surface array by labeling them as fixed terrain type. If all the vertices of a polygon are fixed, a pressure-sinkage relationship for the force calculation is described as a linear function

$$p(z) = K \cdot z, \tag{4}$$

where $K = 1.0$ GPa/m and z is the sinkage. The height values of these fixed points are not changed under load and their sinkage values are returned to zero after the force calculation. The value of K was selected in order to produce large enough forces for realistic modeling of rigid objects, but in a way that it is not producing massive forces with small sinkage values, which could be numerically problematic during the equilibrium search, where the total force and torque affecting the vehicle are minimized.

2.3. *Vehicle–terrain interaction: computational model*

Computational work of the vehicle-terrain interaction can be divided into four distinctive phases. First, the 3D models of wheels and track shoes are converted to the grid defined by the surface array. Thereafter, the points of the terrain under load are identified and the numerical integration of pressure over surface polygons is performed. When forces

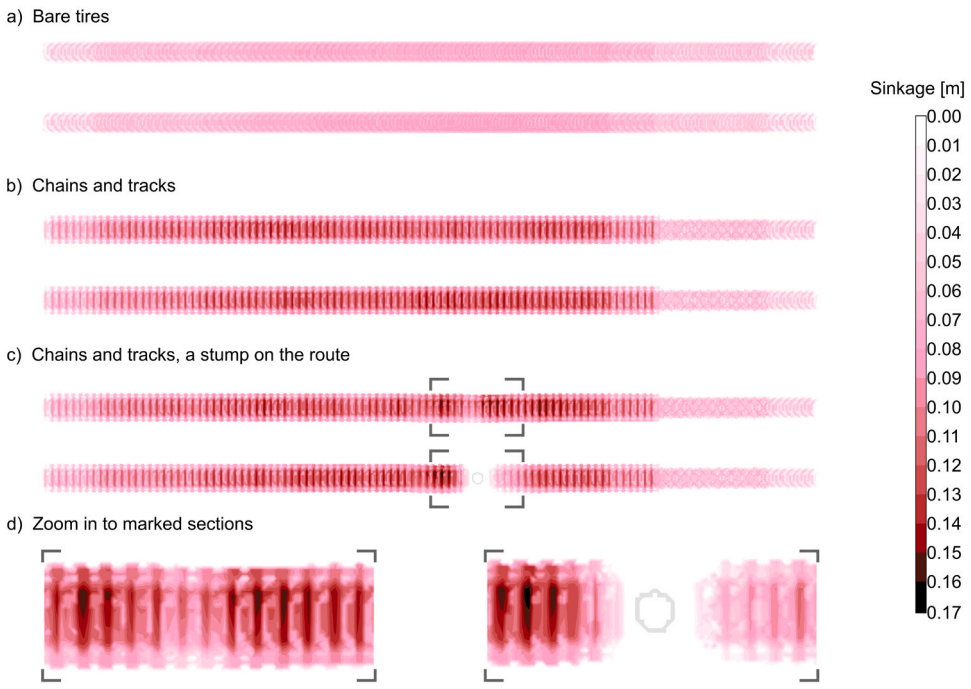

Fig. 11. Top view showing rut depths of the forwarder with different running gear configurations and when run over a stump. The running direction is from left to right.

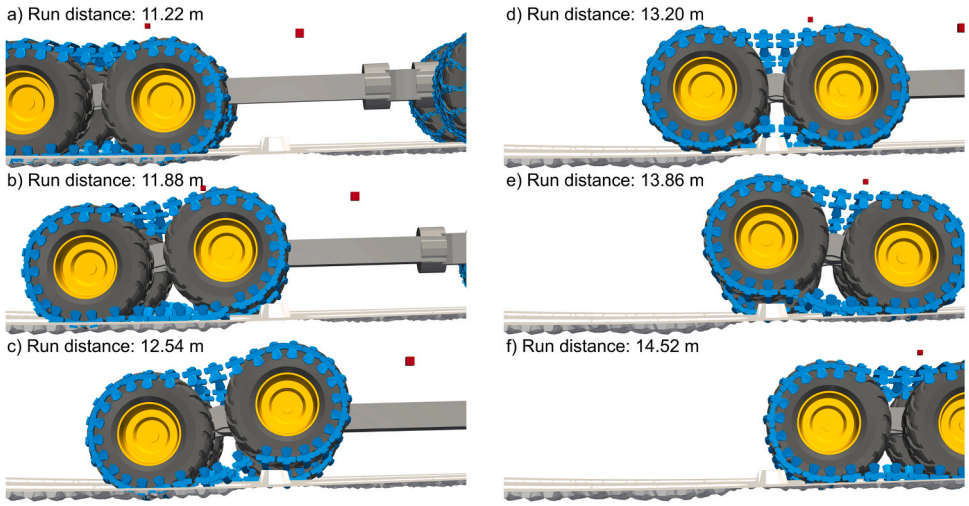

Fig. 12. Visualization of the cut-to-length timber forwarder running over the stump. Red cubes represent centers of mass of the whole vehicle and the rear frame component.

and torques are calculated, the vehicle and its parts will be moved and rotated to iteratively find the equilibrium position with corresponding wheel footprints. The optimized geometry and position of the vehicle is used to modify the terrain surface according to the footprints and the rolling resistance coefficient is calculated.

A set of tests was performed to validate all the computational methods and algorithms described in the following sections. The set is described more in detail and examples of results are presented in the Appendix, section B.

2.3.1. Conversion of vehicle 3D model to terrain grid

Wheels and track shoes are the objects which can be in contact with the terrain. To identify which points on the terrain surface are under pressure the above mentioned objects have to be converted to the grid which is defined by the surface array. The conversion is made by calculating the height of the surface of an object at positions set by the surface grid. The method is illustrated in Fig. 3.

First, the polygon of the object is projected onto the XY-plane and the possible points of the terrain grid inside the projected area are identified. The height of the polygon surface at the identified point position is calculated. If the height value is smaller than the current Z-value of the terrain point, the 3D model is in contact with terrain at that position. The minimum calculated height for each contact point of the terrain surface is stored to form the geometry of the object in a grid space, and this is called the grid model of an object in this article.

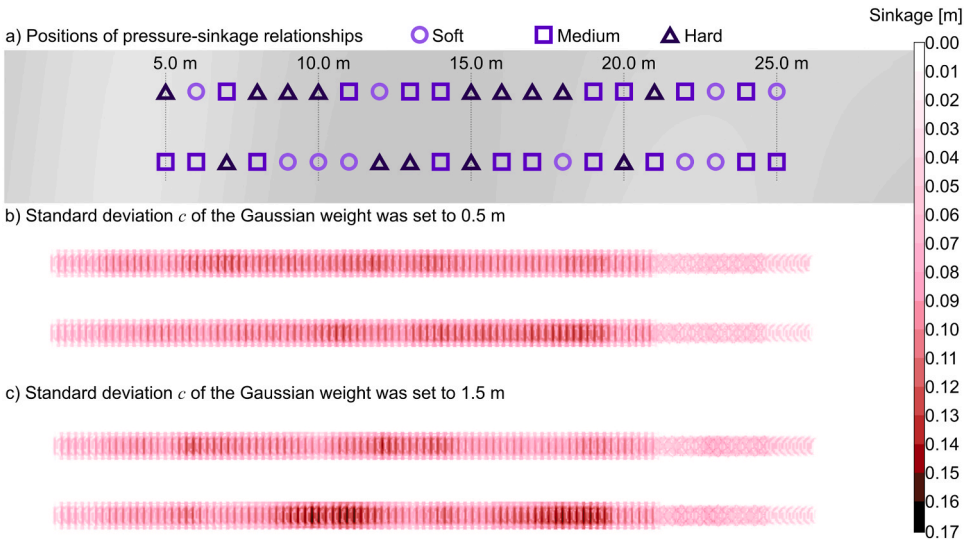

Fig. 13. Top views. a) Locations of varying pressure-sinkage relationships b) Rut depths of the forwarder with chains and tracks, the standard deviation c of the Gaussian weight was set to 0.5 m c) Rut depths of the forwarder with chains and tracks, the standard deviation c of the Gaussian weight was set to 1.5 m. The running direction is from left to right.

2.3.2. Force calculation by numerical integration of pressure over contact area

After the grid model of an object is generated, it can be used to find points on the soil surface which are under pressure. This is done by searching points from the grid model which are at lower elevations than corresponding points in the surface array. When a point under load is found, polygons on which it is acting as a vertex are listed. Numerical integration of pressure is made over these polygons.

Triangular polygons on the surface of the terrain can be represented in two different spaces, the real space with corner height values from the DEM and in the sinkage space where the height values of corners are their sinkage values (relative to the original unperturbed surface). The original orientation, the orientation in a real space after loading (polygon under pressure from a vehicle object) and the loaded polygon in the sinkage space are presented in Fig. 4. There is also a possibility that all the corners of a polygon have a sinkage value ≥ 0, but just some of them are currently under load. This is common for example when the front wheels have already run over a spot and the rear wheels have reached the same area.

If at least one of the corners of a polygon is under a load, the force calculation is performed. Numerical integration of pressure over a polygon is executed with a step-by-step procedure:

2.3.2.1. Elevation and sinkage values of polygon corners. If the elevation value Z of a point in the surface DEM is higher than the corresponding point in the grid model of the object (a wheel or a track shoe), the point in the DEM and accordingly the corner of the surface polygon is considered to be under load. Thus, the Z value of the point in the DEM is set to the level defined by the grid model and the sinkage value for the corner is calculated as the difference from the current elevation Z relative to the original (unperturbed) elevation. Because there is also a possibility that the polygon is only partially under load, the load information of all the corners is also collected. After the force calculation, the elevation and sinkage values of the DEM are returned to the state prior to the force calculation.

2.3.2.2. Division of the surface of a polygon. An integration resolution is set by the user and it defines the number of equal length parts into which the side vectors of a polygon are divided. The polygon is sliced with lines parallel to side vectors. This way the integration resolution R_i will result ${R_i}^2$ subpart triangles with equal area. For example in Fig. 4 b) the integration resolution is 3 and there are 9 subpart triangles. A similar numerical integration method with a subtriangle division was presented by Bartholomew (1959) and has been used for example in a computational geomechanics application by Peres et al. (2021).

2.3.2.3. Calculation of the force of a subpart. The center of a subpart triangle is calculated as an average from (X, Y)-values of the corners. X- and Y-coordinates of the center are used to pick a corresponding sinkage value from the polygon surface in the sinkage space. An average pressure-sinkage relationship vector $\bar{\mathbf{p}}$ is calculated from the pressure-sinkage vectors of polygon vertices. The pressure value for a subpart is got from this vector by linearly interpolating between the vector defined values. A force value for the subpart l is calculated by

$$F_l = p_l \cdot A_{sub}, \tag{5}$$

where p_l is the pressure value for the subpart l and A_{sub} is the area of the subpart.

Polygons may also be partially under load, where one or two of the three vertices are in contact with the vehicle running gear. In this case, the force calculation of a polygon can be limited by integrating over only the area close to the corner or corners under pressure.

A vector with the load information of all the corners of a polygon is passed to a force calculation method. The vector has 0 value designated for corners which are not under load and value 1 for corners currently under load. During the force calculation of a subpart, a barycentric coordinate vector for the center of a subpart is calculated. A load correction value L_c is calculated by

$$L_c = \mathbf{B}_l \cdot \mathbf{U}_{poly}, \tag{6}$$

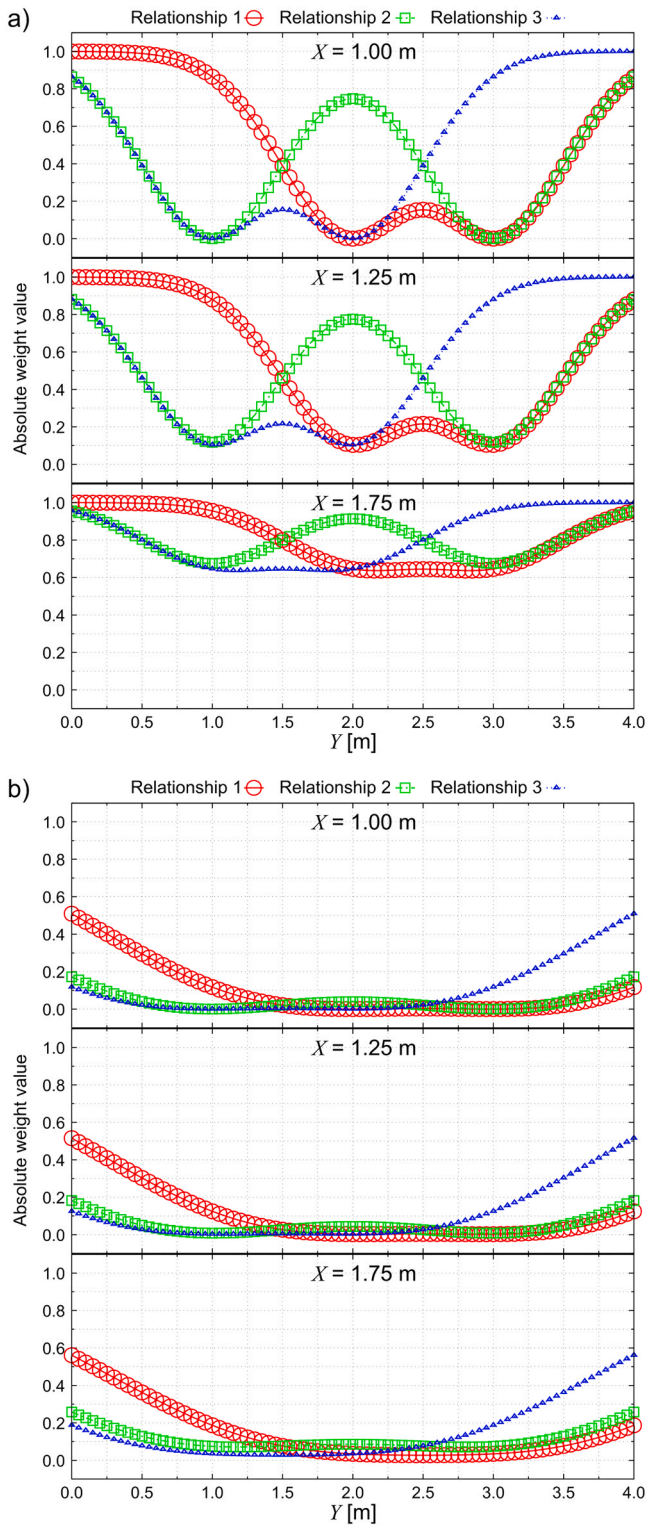

Fig. A1. The absolute weight values of each pressure-sinkage relationship from three cross-sections in Fig. 2. Subfigure a) presents the case with the standard deviation $c = 0.5$ m and b) $c = 1.5$ m.

where $\mathbf{B}_l$ is the barycentric coordinate vector for the subpart l and $\mathbf{U}_{poly}$ is the load information vector for the current terrain polygon. Integration is limited with a simple step function, which sets a multiplier for the calculated force of the subpart. The multiplier is 0.0 for $L_c < 0.5$ and 1.0 for $L_c \geq 0.5$. An example of a polygon with a single corner under load and the corresponding force calculation with the step function limitation is presented in Fig. 5.

2.3.2.4. Force generated by a terrain polygon. The force vector $\mathbf{F}_p$ generated by a polygon is calculated by

$$\mathbf{F}_p = \left(\sum_l F_l\right) \cdot \mathbf{u}, \tag{7}$$

where F_l is the force value of the subpart l and $\mathbf{u}$ is the unit vector to the direction perpendicular to the polygon surface. The position vector $\mathbf{r}_F$ of the force vector $\mathbf{F}_p$ is calculated as a weighted average

$$\mathbf{r}_F = \frac{\sum_l (F_l \cdot \mathbf{r}_l)}{\sum_l F_l}, \tag{8}$$

where $\mathbf{r}_l$ is the position vector of a subpart l in the global coordinates.

2.3.3. Finding the equilibrium

When a vehicle is run over a terrain during the simulation, the equilibrium is searched on every run step. Speed is not taken into account and because of this, the computational method presented here is suitable for vehicles moving with low speed.

Vehicles may have a vast number of degrees of freedom. Tracks, if present, are forming a flexible multi-object group, where track shoes are also affected by forces acting on their neighbors. Thus, their geometry has to be optimized every time the corresponding bogie is moved or rotated. In the next two sections, the optimization methods for tracks and vehicle parts, such as bogies or larger components, are described.

2.3.3.1. Tracks. The positions and angles of track shoes are controlled by the backbone of interconnecting track links, presented in Fig. 1. The accuracy of equilibrium search is controlled by an energy tolerance ϵ_e and a position tolerance ϵ_d. To prevent tracks from slipping on wheels during the optimization, points of the backbone in contact with the top part of each wheel are locked in place.

The optimization of a track geometry is started by calculating forces acting on track shoes. When forces are known, the potential energies of track shoes are calculated. If a track shoe is not interacting with the terrain, its potential energy E_T is calculated

$$E_T = m_T g h_T, \tag{9}$$

where m_T is the mass of a track shoe, $g = 9.81 m/s^2$ and h_T is the height of a center point of a track shoe, calculated as a vertical distance from the surface of the terrain. If the track shoe is interacting with the terrain and thus impacted by a vertical force F_T, the potential energy is approximated as if the terrain would behave like a spring. The spring constant k is calculated from the force by

$$k = \frac{F_T}{z_T}, \tag{10}$$

where z_T is the sinkage of the center point of a track shoe. Then the potential energy of a track shoe is

$$E_T = \frac{1}{2} k {z_T}^2, \tag{11}$$

and the total potential energy of tracks E_{pot} is the sum of potential energies of individual track shoes. From the second optimization step on, the total potential energy and track shoe positions from current step j and previous step $j-1$ are compared. If the absolute value of the difference in potential energy

$$\Delta E = E_{pot,j} - E_{pot,j-1} \tag{12}$$

or the maximum difference from track shoe positions d_{max} are smaller than corresponding tolerances ϵ_e and ϵ_d, the equilibrium of track position is considered to be reached.

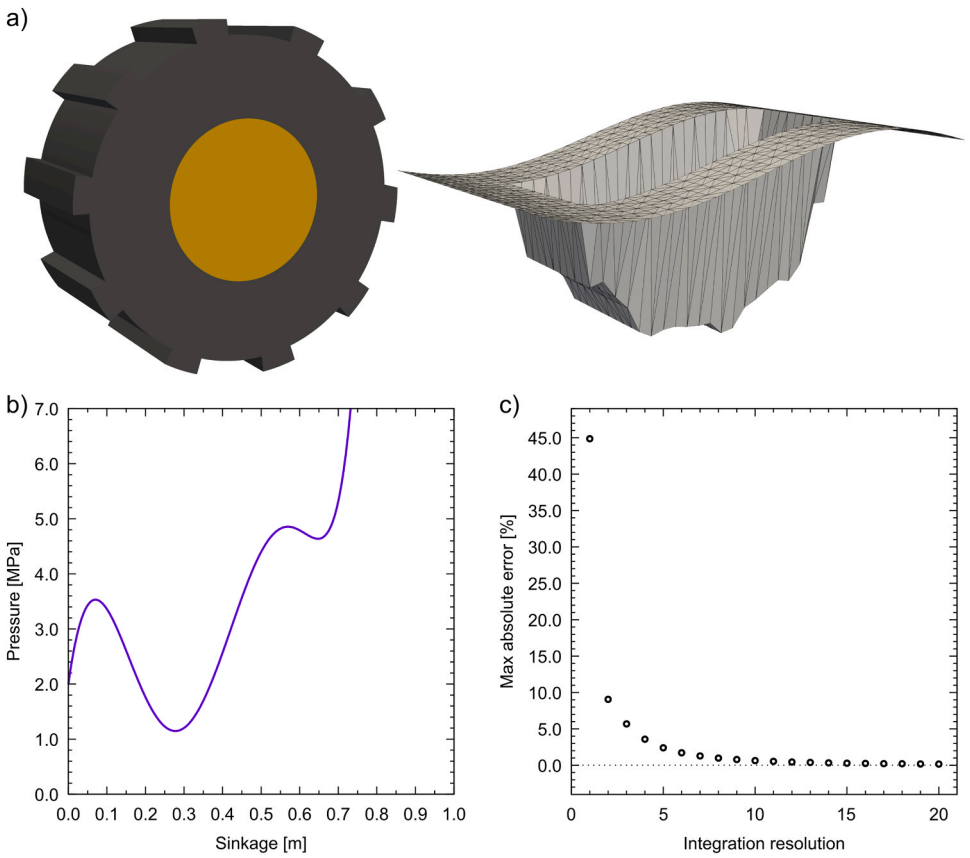

Fig. B1. The force calculation of polygons was tested by pressing terrain with a wheel and computing force value from each modified polygon. Subfigures present: a) the wheel and terrain surface geometry, b) the pressure-sinkage relationship, c) the maximum absolute error between computed and exact values.

If $|\Delta E| > \epsilon_e$ and $|d_{max}| > \epsilon_d$, the positions of track shoes are shifted to form the geometry of the track for the next iteration step and force calculation. For each point of the backbone, a sum force vector is calculated by adding the forces from both track shoes it is interacting with. The projection of the force vector to a plane defined by the bogie geometry is used as a shift direction for the backbone link point. After all the points of the backbone are shifted according to forces acting on them (except points locked on wheels), an iterative process is run to return the distance between points to match the set track link pitch, while preventing points to be placed inside wheel geometries. When the backbone geometry is optimized, the track shoe geometries are shifted and rotated according to joint points. New iteration can be started by calculating new forces.

In addition to a tolerance check, the potential energy is used to adjust the length of the shift which is applied to the link points in each iteration of the equilibrium search. If $\Delta E > 0$, the potential energy increased from the previous iteration and the equilibrium geometry of the track is considered to be between these geometries. Thus, the shift is halved and eventually the equilibrium search converges.

2.3.3.2. Vehicle. The equilibrium of a vehicle is searched by starting the optimization from the smallest segment, usually tracks or bogies with wheels. The optimization of the positions and orientations of these parts results in forces (vectors and their positions) caused by the interaction with the terrain. These forces are passed as an input for the optimization function of a larger section, for example a component. A flow chart of the equilibrium search for the forwarder (visualized in Fig. 1) is presented in Fig. 6.

For example, with the forwarder the first step is to optimize the geometry of tracks, which has an effect to the orientation of the bogie. Forces from the bogie are used for the calculation of the torque acting on the component it is attached to and eventually to calculate the torque and the total force acting on the vehicle.

The accuracy of an optimization can be tuned by tolerances set by the user. When the equilibrium position of the vehicle is found, the surface of the terrain is modified by leaving the wheel (and track) footprint to the current position and resulting forces are used in the rolling resistance coefficient calculation.

2.3.4. Rolling resistance coefficient

The rolling resistance coefficient is defined by the ratio

$$C_{RR} = \frac{F_R}{N}, \tag{13}$$

where F_R is the force needed to make a wheel roll at constant speed over a terrain, and N is the normal force generated by the terrain. During a simulation run, the rolling resistance coefficient is calculated in each step after the equilibrium of the vehicle is found.

2.3.4.1. Rolling resistance coefficient of a wheel. The normal force N for a wheel is

$$N = \left\| \sum_p \mathbf{F}_p \right\|, \tag{14}$$

where $\mathbf{F}_p$ is a force vector from the polygon p. All the force vectors acting on the wheel are known when the search of the equilibrium for the vehicle is concluded. Therefore, to calculate the rolling resistance

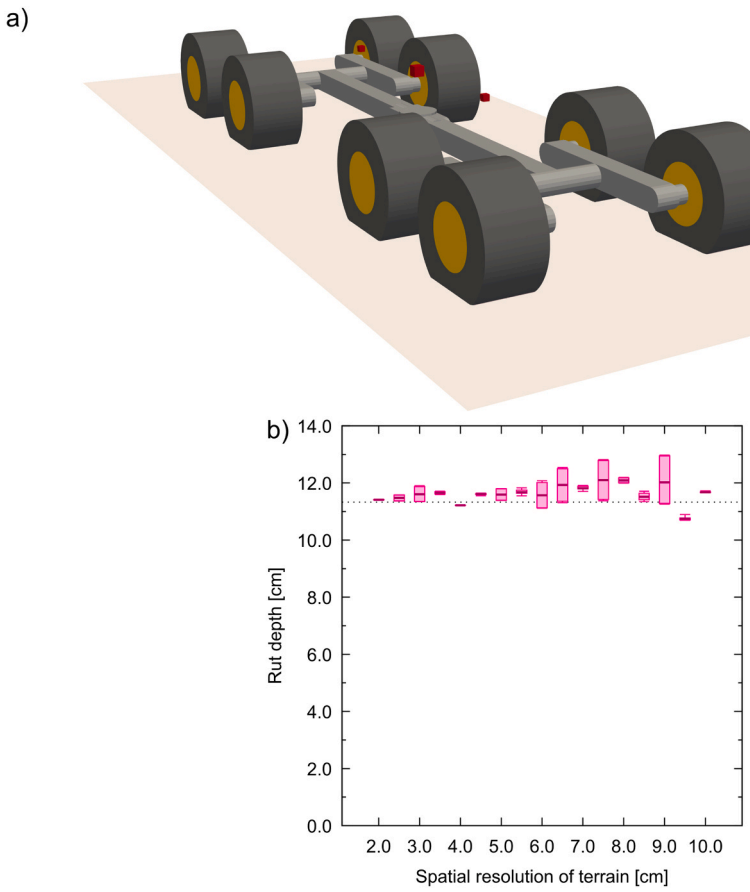

Fig. B2. The equilibrium search and its accuracy on a vehicle consisting rotating components with wheel bogies. Subfigures present: a) the equilibrium state of the vehicle, b) computational rut depth values as the function of a spatial resolution of the terrain and the high accuracy validation value (dashed line).

coefficient of the wheel, the real task is to compute F_R.

The rolling of the wheel over the terrain can be considered as an infinitesimal rotation around a pivot point, which represents a spot directly under the wheel in relationship to the rolling direction (Fig. 7). The rolling direction $\mathbf{r}_d$ is defined as a difference vector

$$\mathbf{r}_d = \frac{(\mathbf{r}_{cc} - \mathbf{r}_{cp})}{\| \mathbf{r}_{cc} - \mathbf{r}_{cp} \|}, \tag{15}$$

where $\mathbf{r}_{cc}$ is the current position vector and $\mathbf{r}_{cp}$ is the previous position vector of the wheel center. The wheel radius vector $\mathbf{R}$ is calculated by rotating the rolling direction vector $\mathbf{r}_d$ 90 degrees around the wheel axle and multiplying it with R, the radius of the wheel. The position vector of the pivot point $\mathbf{r}_{pivot}$ is then

$$\mathbf{r}_{pivot} = \mathbf{r}_{cc} + \mathbf{R}. \tag{16}$$

During the force calculation, all the terrain polygons which are generating a force on the wheel are listed. If the wheel is rolled an infinitesimal amount from the current position, along the rolling direction around the pivot point, each of these forces is considered to cause a torque on the wheel. Polygons in front of the pivot point are resisting wheel movement and polygons behind it are propelling the wheel.

The rolling of the wheel is considered to be caused by the force F_R, which is pointing along the rolling direction and is acting at the center of the wheel. To make the wheel roll at constant speed, the torque generated by the force F_R, has to be equal to the torque generated by the forces of the terrain polygons. This is presented in Fig. 7 and has been previously discussed by Komandi (1999). Hereby F_R is

$$F_R = \frac{\sum_p ((\mathbf{F}_p \times (\mathbf{r}_p - \mathbf{r}_{pivot})) \cdot \mathbf{u}_A)}{R}, \tag{17}$$

where $\mathbf{F}_p$ is a force vector from a terrain polygon, $\mathbf{r}_p$ is the position vector of the force vector and $\mathbf{u}_A$ is a unit vector along the wheel axle (pointing out of the Fig. 7). After the calculation of F_R the rolling resistance coefficient can be calculated with Eq. (13).

2.3.4.2. Rolling resistance coefficient with tracks. Steel tracks are often mounted on the bogie wheels of cut-to-length timber harvesters and forwarders. Bogie tracks are not usually covering the contact surface entirely, but a contact area is a combination from track shoes and wheels. This can be seen at rear bogies of the forwarder presented in Fig. 1.

To overcome this issue and to form a general method for calculation of the rolling resistance coefficient with tracks, the method presented for a single wheel was expanded for tracks. In addition to the forces acting on the wheel generated by the terrain polygons, the forces from tracks are also taken into account in rolling resistance calculation. The method described in this subsection is applicable for vehicles with partially covering bogie tracks (Fig. 7 b) or machinery with fully covering tracks, such as typical military vehicles.

After the optimization of the track geometry, the positions of track shoes and forces acting on them are known. Thus, track shoes in contact with each wheel can be identified. However, a track shoe which is in contact with the wheel surface but whose position is below the axle centerline of the corresponding wheel is not considered to be in contact

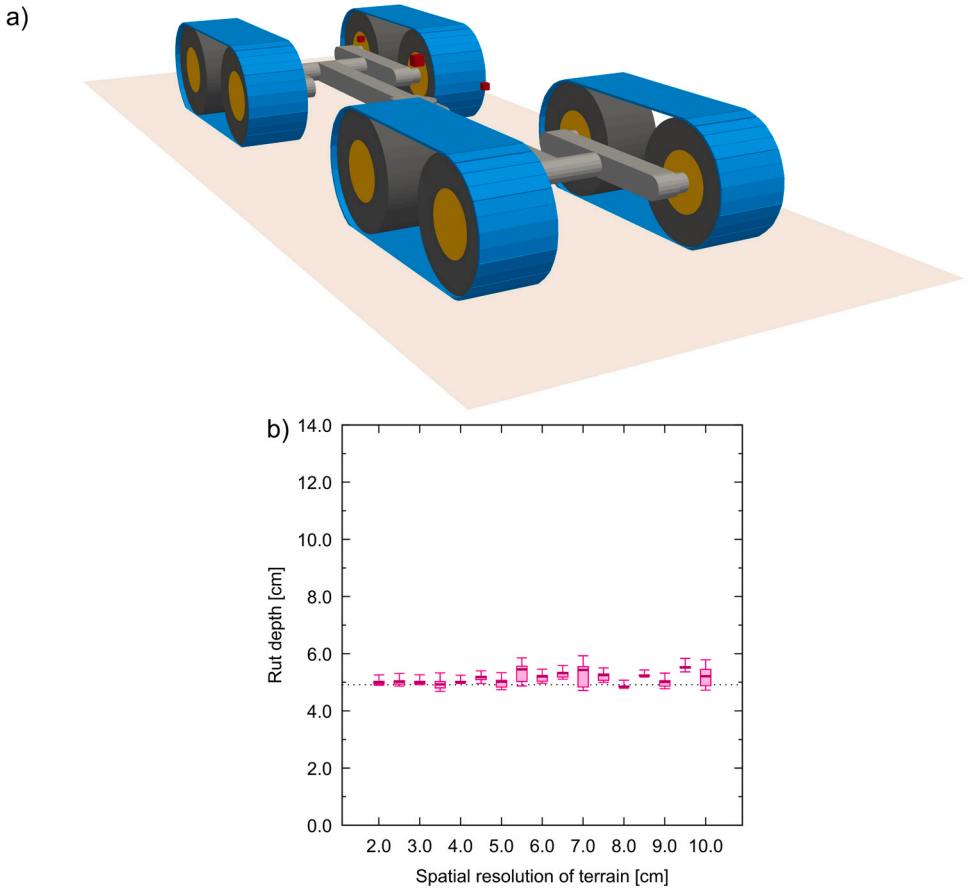

Fig. B3. The equilibrium search and its accuracy on a vehicle consisting rotating components with tracked wheel bogies. Subfigures present: a) the equilibrium state of the vehicle, b) computational rut depth values as the function of a spatial resolution of the terrain and the high accuracy validation value (dashed line).

with the wheel, if the vertical component of the total force acting on it is less than zero, meaning the weight of the track shoe is larger than a vertical force from the terrain. Instead, total forces from these track shoes are designated as the tension forces acting on hanging points presented in Fig. 7 b).

The track sections between the bogie wheels are considered to form flexible multi-object parts, and tension forces at the end points of the sections act on wheels. The direction of each tension force is parallel to the direction of the first non-wheel contact track shoe at that end of the section. The total force vector of the section is calculated by summing the force vectors acting on each track shoe in the section. This total force is then distributed to the section ends according to the vertical component of the tension force vector of each end. These forces are used in the rolling resistance coefficient calculation.

For track shoes in contact with the wheels, the forces acting on each shoe are summed and the position of this total force is set to be the center position of a track shoe. All the forces taken into account for rolling resistance coefficient calculation for a bogie with tracks are presented in Fig. 7 b).

After this the calculation of rolling resistance coefficient simplifies to a single wheel case for each wheel, where same equations (14), (15), (16) and (17) are used. The only difference is that in addition to forces from terrain polygons, the forces calculated from tracks are used.

When rolling and normal forces have been calculated, the total rolling resistance coefficient $C_{RRtotal}$ for a bogie or for a whole vehicle is

$$C_{RRtotal} = \frac{\sum_n F_{Rn}}{\sum_n N_n}, \tag{18}$$

where F_{Rn} and N_n are the rolling and normal force of the wheel n, respectively, and summation is done over all the wheels.

2.4. Running a vehicle over terrain

A vehicle is run over a patch of terrain by setting a desired route and defining a run step, which determines the distance to be moved between the equilibrium searches. In addition, the number of intermediate steps n_i can be set. The run step is divided into $n_i + 1$ intervals and the vehicle is moved according to this intermediate step length. At each intermediate position, a simplified equilibrium search is executed and after this the vehicle geometry is shifted upwards until the total force is less than zero, i.e. the force from the terrain is smaller than the weight of the vehicle. Wheel and track footprints are generated in these positions. This approach corrects the effect caused by the finite run step length and provides convergence of the rut depth and the rolling resistance coefficient as the function of the spatial resolution of the terrain. Also, it prevents unrealistic sinking of the vehicle on plastic terrains. A schematic image about the effect of intermediate steps to a rut depth with a single wheel running over the terrain is shown in Fig. 8.

The spatial resolution of the terrain defines the lower limit of the run step. To ensure that there are always new terrain polygons under load when the equilibrium of the vehicle is searched, the lower limit of the run step is $\sqrt{2} \cdot d_t$, where d_t is the spatial resolution of the terrain surface. Both integer parameters, the number of intermediate steps and the integration resolution, are coupled to their parent parameters, the spatial resolution of the terrain and the run step, and their applicable minimum values can be checked via convergence calculations when the aforementioned parameters have been set.

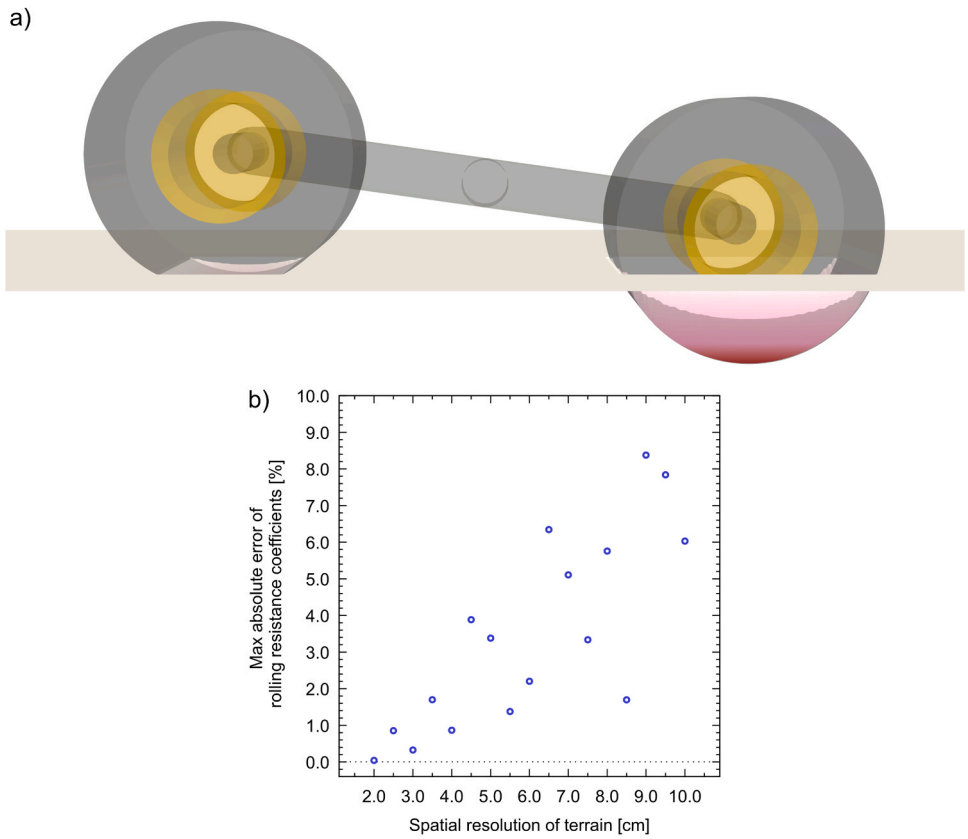

Fig. B4. The computation of a rolling resistance coefficient was tested by setting a bogie with wheels on the flat surface of a terrain. Subfigures present: a) the geometry of a simulation, b) the maximum of an absolute error between the rolling resistance coefficient calculated by VieteriSim software and the high accuracy validation value as the function of a spatial resolution of the terrain.

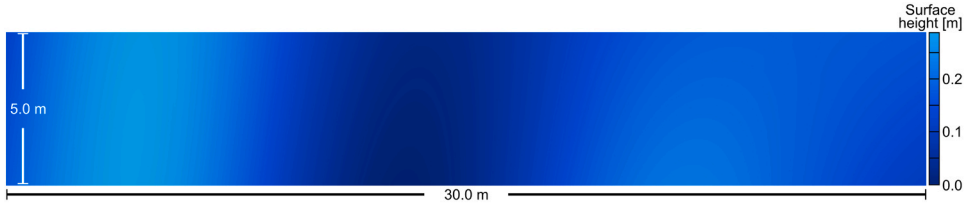

Fig. C1. Top view showing the surface and dimensions of the testing terrain in simulations.

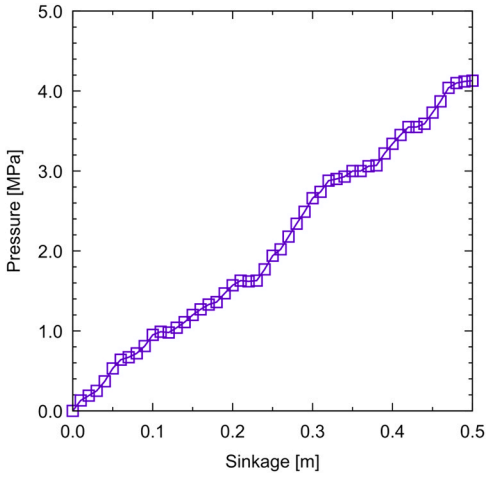

Fig. C2. The pressure-sinkage relationship of the terrain in convergence tests and in simulations with a uniform relationship on the area.

2.5. Simulations for convergence test

The convergence of ISCM and the performance of the simulator was examined by running a series of simulations. The rut depth and the rolling resistance coefficient should converge when the spatial resolution of the terrain is decreased.

The vehicle run in convergence tests was a modeled to represent Ponsse Elk cut-to-length timber forwarder (Ponsse Plc, Vieremä, Finland), presented in Sec. 2.1. Two separate vehicle configurations were applied. The first configuration was run with the bare rubber tires. The second setup had chains on the rear wheels of the front bogies and Olofsfors Evo Soft tracks on the rear bogies (Olofsfors AB, Nordmaling, Sweden), as presented in Fig. 1. In both cases a load of 6500 kg (50 % of the total capacity) was set to the forwarder, bringing the total mass of the vehicle to 27445 kg when equipped with chains and tracks.

The surface geometry of the terrain was generated in the simulator by adding two sinusoidal modifiers to a flat surface. Thus the final surface had height variation of approximately 30 cm. The pressure-sinkage relationship of the terrain was constructed from a linear function with added random noise. The behavior of the simulated terrain was

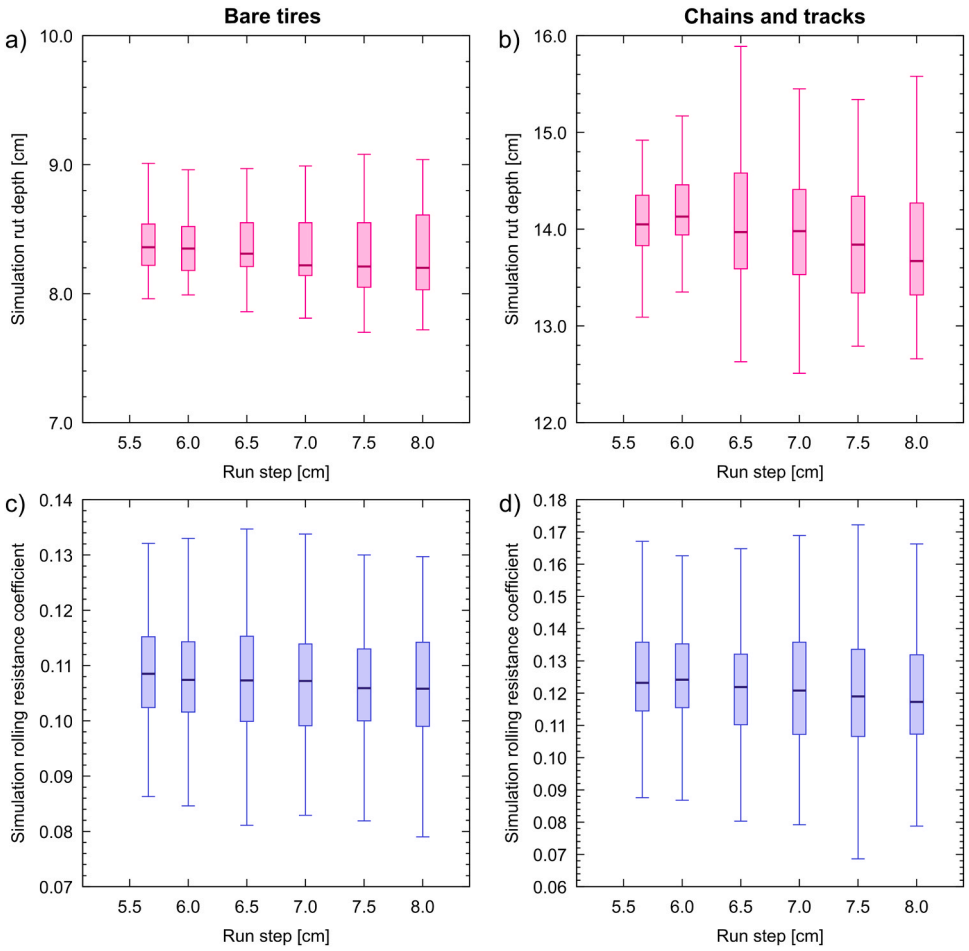

Fig. D1. Distributions of rut depth and rolling resistance coefficient for the Ponsse Elk forwarder (the spatial resolution of the terrain is 4.0 cm, the number of intermediate steps is 25, the integration resolution is 12), the run step value for a simulation is in the 5.66–8.0 cm range. Values for the configuration running on bare wheels are presented in a) and c) and the configuration with chains and tracks in b) and d). The length of the run step was increased to check the convergence limit.

plastic. Thus, the final sinkage values of the terrain surface represent rut depths at corresponding locations. Visualizations of the surface of the terrain and the pressure-sinkage relationship are presented in the Appendix, section C.

In the first set of simulations, the number of intermediate steps was set to 25 and the integration resolution was 12. These values were large enough not to limit simulation accuracy. The spatial resolution for the terrain was increased from 2.5 cm to 7.0 cm and the run step was the minimum value $\sqrt{2}\cdot d_t$ for each resolution. We found the maximum spatial resolution, where the simulation could be still considered to be converged. Then similar simulation sets were run to check the convergence limits for the run step, the number of intermediate steps and the integration resolution.

The total length of the vehicle is approximately 8 m. To ensure a 10 m long segment of terrain, where all the wheel pairs had trafficked the terrain and the final rut depths could be measured, the vehicle was run on a surface for 18 m. For data analysis, rolling resistance coefficient values were collected from steps on the last 10 m of the run. Rut depths were measured in the left and right tracks by sampling the rut with a 25 cm long window and taking the maximum sinkage in the window as the rut depth value. A total of 80 rut depth values were acquired for each run. The simulation area, the section of the run where rolling resistance coefficient values are collected, and sectors for measuring rut depths are visualized in Fig. 9.

3. Results

Distributions of rut depth and rolling resistance coefficient values for both vehicle configurations (bare tires or chains and tracks) on terrain surfaces with spatial resolution values in the 2.5 – 7.0 cm range are presented in Fig. 10. The whiskers of each box plot was set to the minimum and maximum values of a range which is 1.5 times the interquartile range.

ISCM presents convergence of rut depth and rolling resistance coefficient values with both vehicle configurations when the spatial resolution of the terrain is decreased sufficiently. The spatial resolution of 4.0 cm, providing the convergence of results while maintaining a manageable computational load, was selected for simulations.

To further ease the computational load, while maintaining the convergence of results, tests similar to those conducted with spatial resolution, were made for the run step, the number of intermediate steps and the integration resolution. Results of these are shown in the Appendix, section D. As a result of the convergence tests, the final parameters for simulations were: 4.0 cm spatial resolution, 6.0 cm run step, 21 intermediate steps and 4 as integration resolution.

By using the selected parameters, the Ponsse Elk forwarder with bare tires, chains and tracks, was simulated running over a 35 cm wide and 15 cm tall stump. The terrain surface topography and the pressure sinkage relationship were the same as those used in the convergence tests. Rut depths (sinkage values) from simulation runs are visualized in Fig. 11.

Because of terrain plasticity and an increase in the total vehicle

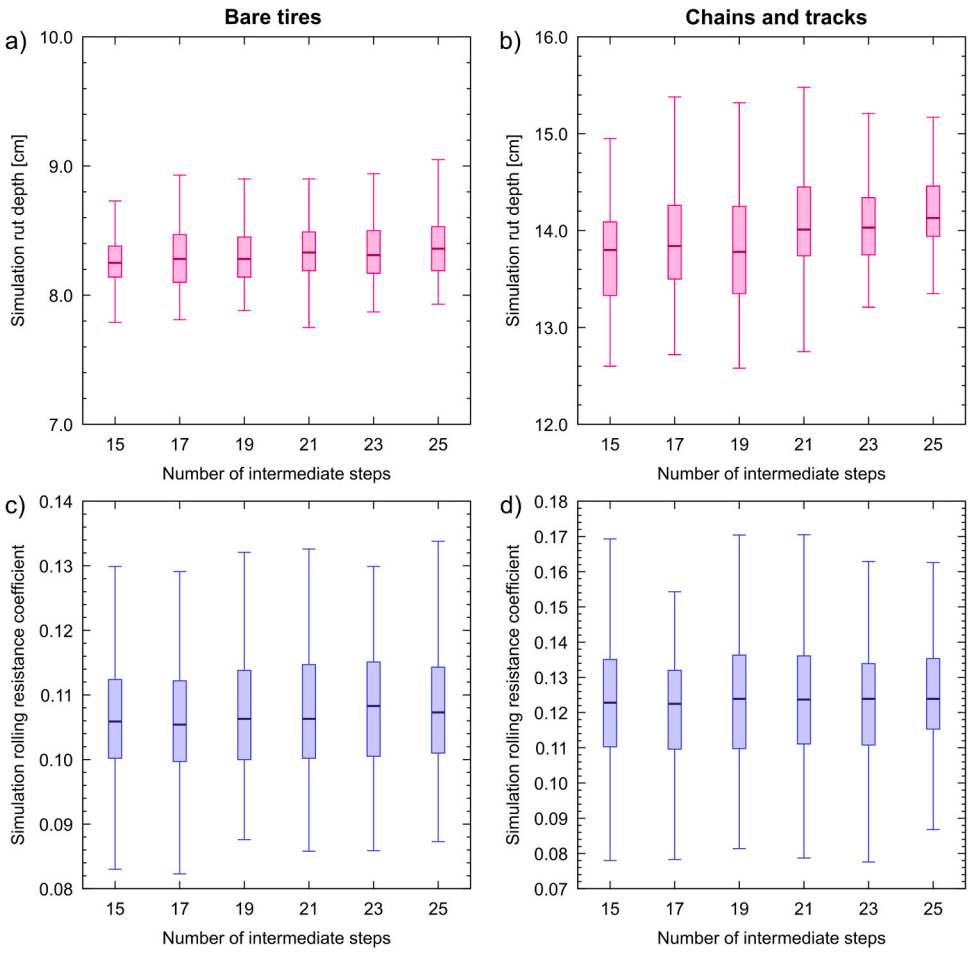

Fig. D2. Distributions of rut depth and rolling resistance coefficient for the Ponsse Elk forwarder (the spatial resolution of the terrain is 4.0 cm, the run step is 6.0 cm, the integration resolution is 12), the range of the number of the intermediate steps for a simulation is 15–25. Values for the configuration running on bare wheels are presented in a) and c) and the configuration with chains and tracks in b) and d). The number of the intermediate steps was decreased to check the convergence limit.

weight, routes run with the configuration featuring chains and tracks, have deeper ruts. In addition, the visualized route from the simulated run over the stump, presents deeper ruts next to the stump on the right and the left track in comparison to the simulation without rigid obstacles. Hereby, the simulation replicates realistically the forwarder climbing on and over the stump, while leaning to the left. The tilting of the vehicle can be observed also from deeper ruts pressed by the left hand halves of both left and right track shoes, clearly visible on zoomed in sections shown in Fig. 11 d).

A closer look to the geometry of tracks and the forwarder running over the stump is presented in Fig. 12. The visualization shows that the track optimization algorithm provides realistic track geometry through the run over of the stump. Tracks are hanging loosely when only one of the wheels is on top of the rigid stump, as presented in Fig. 12 b), c) and e). Fig. 12 d) shows the moment during the bogie trafficking the stump, when only the track is supporting the bogie.

The effect of the standard deviation, c, of the Gaussian weight for the pressure-sinkage relationship array generation was also tested. The same forwarder with chains and tracks was simulated on the same terrain topography as in previous examples, but the pressure-sinkage relationship array of the terrain was formed from 42 pressure-sinkage relationships with three different overall strengths; soft, medium and hard. Positions of pressure-sinkage relationships are presented in Fig. 13 a). The "Medium" relationship is the same one which was used in convergence tests and in rut depth simulations whose results are shown in Fig. 11. All three pressure-sinkage relationships are visualized in the Appendix, section E. Two different values for the standard deviation c were used, 0.5 m and 1.5 m. Fig. 13 b) shows that with $c = 0.5$ m the effect of an individual relationship is diminutive. However, with $c = 1.5$ m, soft and hard areas along the route are clearly visible in rut depth values.

4. Conclusions

An integration soil contact model provides a flexible and accurate method for force calculation when simulating a vehicle moving with low speed on a soft terrain. The pressure-sinkage relationship of each simulation can be freely defined by a function or an experimental data set and may be varied spatially. The model and the presented Vehicle-Terrain Interaction Simulator software, VieteriSim, are applicable for simulating vehicles running on wheels or tracks, and they handle rigid objects on the terrain, such as rocks and stumps.

VieteriSim and the equilibrium search algorithms discussed in this article, produce realistic behavior for a vehicle running on a soft terrain, and even for extreme cases, for example running over a stump, when tracks are in tension. The vector-based rolling resistance coefficient calculation presents a general method which can be used for wheels and tracks with complicated geometries.

The integration soil contact model (ISCM) presents convergence of rut depth and rolling resistance coefficient values relative to the spatial resolution of the terrain. When forces from the terrain and the equilibrium geometry and position of the vehicle are calculated with high accuracy, the convergence of simulated rut depths, when compared to experimental measurements, depends on defining the pressure-sinkage

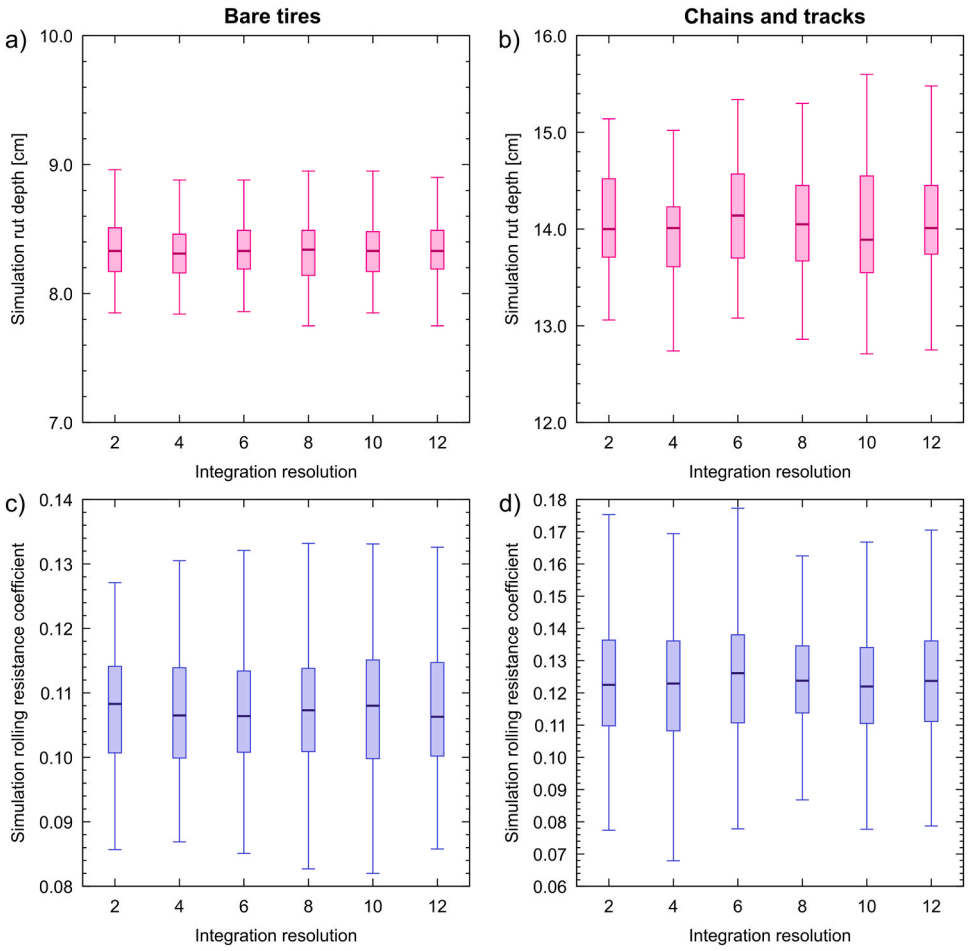

Fig. D3. Distributions of rut depth and rolling resistance coefficient for the Ponsse Elk forwarder (the spatial resolution of the terrain is 4.0 cm, the run step is 6.0 cm, the number of intermediate steps is 21), the range of integration resolution for a simulation is 2–12. Values for the configuration running on bare wheels are presented in a) and c) and the configuration with chains and tracks in b) and d). The integration resolution was decreased to check the convergence limit.

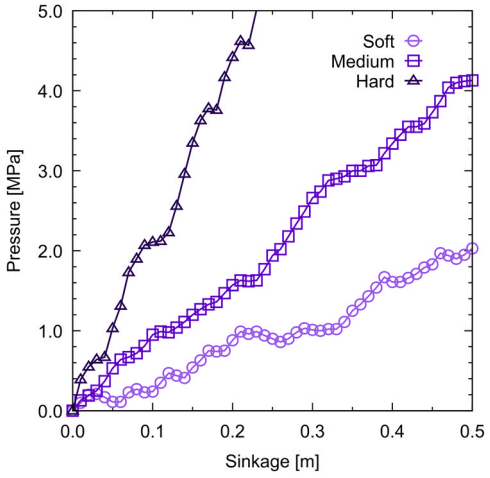

Fig. E1. Pressure-sinkage relationships with three different strengths; soft, medium and hard.

relationship accurately. Our next article will concentrate on pressure-sinkage relationships based on experimental data and validation of ISCM results compared to field test results.

CRediT authorship contribution statement

J. Ala-Ilomäki: Writing – review & editing, Validation, Investigation. **S. Kulju:** Writing – original draft, Visualization, Validation, Software, Methodology, Formal analysis, Conceptualization.

Declaration of Competing Interest

The authors declare that they have no known competing financial interests or personal relationships that could have appeared to influence the work reported in this paper.

Data availability

Data will be made available on request.

Acknowledgments

The research was funded by the Research Council of Finland [grant numbers 295337 FOTETRAF, 332172 TRAM]. We would like to thank Ponsse Plc for providing information on cut-to-length timber harvesters and forwarders, as well as Metsätyö Plc about details of equipment such as chains and tracks. Dr. Samuli Launiainen, Dr. Aura Salmivaara, Dr. Eero Holmström, Mr. Harri Lindeman and Prof. Leena Finér from Luke are acknowledged for their support and prolific discussions during the project.

Appendix A. Absolute weight values

Fig. A1 illustrates the absolute weight values of each pressure-sinkage relationship from three cross-sections in Fig. 2. Subfigure a) presents the case with the standard deviation $c = 0.5$ m and b) $c = 1.5$ m.

Appendix B. Tests

The computational method and algorithms of the simulator were tested, and can be tested in the future, by running a test set consisting 25 tests. In the first two tests, results from the computational integration method were compared to exact values calculated by integrating a polynomial function representing a pressure-sinkage relationship over polygon areas. In tests where computation of rut depth and rolling resistance coefficient values were validated, geometries of wheels where set to be perfect cylinders. Thus, high accuracy validation values could be calculated by simple auxiliary functions. Tests in the set are:

1. **Polygon force calculation**: The integration method is tested by calculating force values over multiple polygons and comparing results to the exact counterparts.
2. **Polygon force calculation, partial load**: The integration method is tested by calculating force values over multiple polygons under a partial load (only one or two vertices are under load) and comparing results to the exact counterparts.
3. **3D model to a terrain grid**: Testing the conversion of a 3D model to the grid defined by the terrain surface array.
4. **Torque of a bogie**: Testing the calculation of the torque of a bogie, compared to a high accuracy validation value.
5. **Search the equilibrium of a bogie according to torque**: A bogie is set to slope with a known angle, the angle of the bogie should be the same as the slope.
6. **Rut depth of a bogie**: The rut depth of a bogie with a load is compared to a high accuracy validation value.
7. **Axis and angles of a vehicle**: Testing the axis and angles of a vehicle after a rotation.
8. **Drive direction**: Testing the drive direction angle of a vehicle.
9. **Start position search**: A simplified equilibrium search of a vehicle, used for a starting position search. The result of the start position search is compared to the normal equilibrium search.
10. **Rut depth of a fixed frame vehicle with wheels**: The rut depth of a fixed frame vehicle with wheels is compared to a high accuracy validation value.
11. **Rut depth of a fixed frame vehicle with wheels on bogies**: The rut depth of a fixed frame vehicle with wheels on bogies is compared to a high accuracy validation value.
12. **Rut depth of a component frame vehicle with wheels on bogies**: The rut depth of a component frame vehicle with wheels on bogies is compared to a high accuracy validation value.
13. **Rut depth of a component frame vehicle with wheels on bogies, off center load**: The rut depth of a component frame vehicle with wheels on bogies, the center of mass is shifted off from the central axis. Effect on rut depths is monitored.
14. **Rut depth of a component frame vehicle with wheels on bogies, on a slope**: The rut depth of a component frame vehicle with wheels on bogies on the terrain with a slope, the center of mass is shifted upwards. Effect on rut depths is monitored.
15. **Rut depth of a fixed frame vehicle with wheels, on a slope**: The rut depth of a fixed frame vehicle with wheels on the terrain with a slope, the center of mass is shifted upwards. Effect on rut depths is monitored.
16. **Rut depth of a component frame vehicle with tracks on bogies**: The rut depth of a component frame vehicle with tracks on bogies is compared to a high accuracy validation value.
17. **Intermediate step optimization**: A simplified equilibrium search of a vehicle performed at intermediate steps of a vehicle run.
18. **Rigid objects**: Testing a stump and a rock, when they are driven over by wheels and tracks. Geometry and sinkage related values on rigid objects should not change.
19. **Rolling resistance coefficient, a bogie with wheels**: The calculation of the rolling resistance coefficient of a wheel is tested by comparing to a high accuracy validation value.
20. **Variance of a rolling resistance coefficient, a bogie with wheels running on terrain**: The variance of the rolling resistance coefficient of a wheel is tested by running a bogie on the surface of a terrain.
21. **Rolling resistance coefficient, a bogie with tracks**: The calculation of the rolling resistance coefficient of a wheel in a bogie covered by tracks is tested by comparing to a high accuracy validation value and monitoring rolling resistance coefficients when the bogie is run on the surface of a terrain and the mass of tracks is increased.
22. **Drive direction dependency of rolling resistance coefficient and rut depth, a wheeled vehicle**: The test is run to check that there is no drive direction dependency on rolling resistance coefficient calculation or rut depths of a wheeled vehicle running on a terrain.
23. **Drive direction dependency of rolling resistance coefficient and rut depth, a tracked vehicle**: The test is run to check that there is no drive direction dependency on rolling resistance coefficient calculation or rut depths of a tracked vehicle running on a terrain.
24. **Pressure-sinkage relationship, read from a data file**: Pressure-sinkage relationships for grid points in a surface array are generated according to the points given in a data file and with various weight functions. The generated pressure-sinkage relationships are checked.
25. **Write and read a restart file**: A vehicle with wheels and tracks is run over a terrain. A restart file is generated in the middle of a simulation run. Results from the original run and a restarted run are compared to check the writing and reading functions of the restart file.

Test examples

In the following, we present four test cases in more detail to exemplify the test set.

Test 1: Polygon force calculation

The force calculation of polygons was tested by pressing terrain with a wheel (presented in Fig. B1 a) and computing force value from each modified polygon. A modified terrain surface and polygons are presented in Fig. B1 a). During the force calculation, all polygons were considered to be fully under load (all vertices are under load). The pressure-sinkage relationship was set to be an eight degree polynomial and is presented in Fig. B1 b). By integrating the pressure defined by the polynomial over a surface polygon, the exact validation value for a force was calculated. Fig. B1 c) presents the maximum absolute error between a computational force calculated by VieteriSim software and the exact value as the function of an integration resolution.

Test 12: Rut depth of a component frame vehicle with wheels on bogies

The equilibrium search of a vehicle was tested by computing the rut depth of a vehicle consisting rotating components with wheel bogies. The radius and width of wheels were set to 0.5 m. The total mass of the vehicle was 30000 kg. The pressure-sinkage relationship of a terrain was a linear function with a slope of 1.5 MPa/m. The surface of the terrain was perfectly flat. An initial position of the vehicle was searched with a

start position search function and a normal equilibrium search was used for the final optimization. The high accuracy validation value was calculated with a simple auxiliary function computing a force acting on a cylinder (have same dimensions as wheels) as a function of sinkage. By multiplying this force value by eight (the number of wheels), the total force and the rut depth of the vehicle could be calculated. With vehicle and terrain parameters defined in this example, the validation value was 0.113224 m. Fig. B2 a) shows the equilibrium state of the vehicle and the subfigure b) presents computational rut depth values as the function of the spatial resolution of the terrain and the high accuracy validation value (visualized with dashed line).

Test 16: Rut depth of a component frame vehicle with tracks on bogies

The equilibrium search of a vehicle was tested by computing the rut depth of a vehicle consisting rotating components with tracked wheel bogies. The radius and width of wheels were set to 0.5 m. The total mass of the vehicle was 32400 kg. The vehicle was identical to Test 12, except the tracks with the total mass of 600 kg each (60 track shoes, 10 kg each), 0.60 m width and a tight setup. The pressure-sinkage relationship of a terrain was a linear function with a slope of 1.5 MPa/m. The surface of the terrain was perfectly flat. An initial position of the vehicle was searched with a start position search function and a normal equilibrium search was used for the final optimization. A high accuracy validation value was calculated with a simple auxiliary function computing a force acting on a cylinder (the radius was the radius of the wheel plus the height of the track shoe, total of 0.52 m, and the width was the width of the track shoe) as a function of sinkage. In addition a force was also calculated as the function of sinkage for a rectangular area with the track shoe width and twice the length of a bogie lever (total of 1.5 m). By multiplying this force value by four (the number of bogies), the total force and the rut depth of the vehicle could be calculated. With vehicle and terrain parameters defined in this example, the validation value was 0.049128 m. Fig. B3 a) shows the equilibrium state of the vehicle and the subfigure b) presents computational rut depth values as the function of the spatial resolution of the terrain and the high accuracy validation value (visualized with dashed line).

Test 19: Rolling resistance coefficient, a bogie with wheels

The computation of a rolling resistance coefficient was tested by setting a bogie with wheels on the flat surface of a terrain. The bogie was rotated by 8.0 degrees and rolling direction was considered to be the direction defined by the bogie (8.0 degrees down from the horizontal level). The geometry of a simulation is presented in Fig. B4. A high accuracy validation value was calculated with a simple auxiliary function computing a force acting on a cylinder (have same dimensions as wheels) as a function of sinkage. Torques according to the pivot point and the rolling resistance coefficient for each wheel were calculated (as described in the article section 2.3.4). The maximum of an absolute error between the rolling resistance coefficient calculated by VieteriSim software and the high accuracy validation value as the function of a spatial resolution of the terrain is presented in Fig. B4.

Appendix C. Terrain in simulations

The surface and dimensions of the terrain in simulations are presented in Fig. C1.

The pressure-sinkage relationship of the terrain in convergence tests and in simulations with a uniform relationship on the area is presented in Fig. C2.

Appendix D. Convergence limit

The results of convergence test simulations for the length of the run step, the number of intermediate steps and the integration resolution are presented in Figs. D1, D2 and D3.

Appendix E. Varied pressure-sinkage relationship

Pressure-sinkage relationships with three different strengths; soft, medium and hard, are presented in Fig. E1.

References

Agarwal, S., Senatore, C., Zhang, T., Kingsbury, M., Iagnemma, K., Goldman, D.I., Kamrin, K., 2019. Modeling of the interaction of rigid wheels with dry granular media. J. Terra 85, 1–14. https://doi.org/10.1016/j.jterra.2019.06.001.

Ahrens, J., Geveci, B., Law, C., 2005. ParaView: An End-User Tool for Large Data Visualization. Visualization Handbook. Elsevier.

Bartholomew, G.E., 1959. Numerical integration over the triangle. Math. Comput. 13, 295–298. https://doi.org/10.1090/S0025-5718-1959-0107976-5.

Bekker, M.G., 1969. Introduction to Terrain-Vehicle Systems. University of Michigan Press, Ann Arbor, Mich., USA.

El-Sayegh, Z., El-Gindy, M., Johansson, I., Öijer, F., 2020. Development and validation of off-road tire-gravelly soil interaction using advanced computational techniques. J. Terra 91. https://doi.org/10.1016/j.jterra.2020.05.004.

Johnson, J.B., Kulchitsky, A.V., Duvoy, P., Iagnemma, K., Senatore, C., Arvidson, R.E., Moore, J., 2015. Discrete element method simulations of Mars Exploration Rover wheel performance. J. Terra 62, 31–40. https://doi.org/10.1016/j.jterra.2015.02.004.

Keller, T., Arvidsson, J., 2016. A model for prediction of vertical stress distribution near the soil surface below rubber-tracked undercarriage systems fitted on agricultural vehicles. Soil Tillage Res. 155, 116–123. https://doi.org/10.1016/j.still.2015.07.014.

Keller, T., Berli, M., Ruiz, S., Lamandé, M., Arvidsson, J., Schjønning, P., Selvadurai, A.P. S., 2014. Transmission of vertical soil stress under agricultural tyres: comparing measurements with simulations. Soil Tillage Res. 140, 106–117. https://doi.org/10.1016/j.still.2014.03.001.

Klaes, B., Struck, J., Schneider, R., Schüler, G., 2016. Middle-term effects after timber harvesting with heavy machinery on a fine-textured forest soil. Eur. J. For. Res. 135, 1083–1095. https://doi.org/10.1007/s10342-016-0995-2.

Komandi, G., 1999. An evaluation of the concept of rolling resistance. J. Terra 36, 159–166. https://doi.org/10.1016/S0022-4898(99)00005-1.

Kurjenluoma, J., Alakukku, L., Ahokas, J., 2009. Rolling resistance and rut formation by implement tyres on tilled clay soil. J. Terra 46, 267–275. https://doi.org/10.1016/j.jterra.2009.07.002.

Lamandé, M., Schjønning, P., 2011. Transmission of vertical stress in a real soil profile. Part I: site description, evaluation of the Söhne model, and the effect of topsoil tillage. Soil Tillage Res. 114, 57–70. https://doi.org/10.1016/j.still.2011.05.004.

Li, H., Schindler, C., 2013. Analysis of soil compaction and tire mobility with finite element method. Proc. Inst. Mech. Eng. Part K: J. Multi-body Dyn. 227, 275–291. https://doi.org/10.1177/1464419313486627.

Li, L., Sandu, C., 2007. On the impact of cargo weight, vehicle parameters, and terrain characteristics on the prediction of traction for off-road vehicles. J. Terra 44, 221–238. https://doi.org/10.1016/j.jterra.2007.04.002.

Meirion-Griffith, G., Spenko, M., 2013. A pressure-sinkage model for small-diameter wheels on compactive, deformable terrain. J. Terra 50, 37–44. https://doi.org/10.1016/j.jterra.2012.05.003.

Peres, M.L., Mesquita, L.C., Leroy, Y.M., Sotelino, E.D., 2021. Stress evolution in elastically heterogeneous and non-linear fluid-saturated media with a Green's function approach. Int. J. Numer. Anal. Methods Geomech. 45, 1323–1346. https://doi.org/10.1002/nag.3204.

Perkins, N., Ma, Z.D., 2002. A track-wheel-terrain interaction model for dynamic simulation of tracked vehicles. Veh. Syst. Dyn. 37, 401–421. https://doi.org/10.1076/vesd.37.6.401.3522.

Salmivaara, A., Miettinen, M., Finér, L., Launiainen, S., Korpunen, H., Tuominen, S., Heikkonen, J., Nevalainen, P., Sirén, M., Ala-Ilomäki, J., Uusitalo, J., 2018. Wheel rut measurements by forest machine-mounted LiDAR sensors - accuracy and potential for operational applications? Int. J. For. Eng. 29, 41–52. https://doi.org/10.1080/14942119.2018.1419677.

Schäfer, B., Gibbesch, A., Krenn, R., Rebele, B., 2010. Planetary rover mobility simulation on soft and uneven terrain. Veh. Syst. Dyn. 48, 149–169. https://doi.org/10.1080/00423110903243224.

Schroeder, W., Martin, K., Lorensen, B., 2006. The Visualization Toolkit, 4th ed. Kitware.

Smith, W., Melanz, D., Senatore, C., Iagnemma, K., Peng, H., 2014. Comparison of discrete element method and traditional modeling methods for steady-state wheel-terrain interaction of small vehicles. J. Terra 56. https://doi.org/10.1016/j.jterra.2014.08.004.

Taheri, S., Sandu, C., Taheri, S., Pinto, E., Gorsich, D., 2015. A technical survey on Terramechanics models for tire-terrain interaction used in modeling and simulation of wheeled vehicles. J. Terra 57, 1–22. https://doi.org/10.1016/j.jterra.2014.08.003.

Wakui, F., Terumichi, Y., 2011. Numerical simulation of tire behavior on soft ground. J. Syst. Des. Dyn. 5, 486–500. https://doi.org/10.1299/jsdd.5.486.

Zhou, F., Arvidson, R.E., Bennett, K., Trease, B., Lindemann, R., Bellutta, P., Iagnemma, K., Senatore, C., 2014. Simulations of mars rover traverses. J. Field Robot. 31, 141–160. https://doi.org/10.1002/rob.21483.